Modelling an Orthotropic Material by an Assemblage of Isotropic Components

John Coffey, Cheshire, UK.

2012

Key words: plywood plates, finite element models, LISA 7 FEA program, resonant modes and frequencies, Chladni figures, comparison of models with experiment.

1 The problem to be addressed

I came across this problem in the course of using the finite element analysis (FEA) program LISA-7 to model the vibration of wooden plates, such as are used as the top and back plates of a violin. LISA is a low price yet powerful FEA program capable of static and dynamic mechanical analysis, plus physical modelling of heat conduction, electric and magnetic fields, etc. Because LISA is relatively easy to use, it has been my choice to introduce myself to FEA as part of a personal interest project to investigate the acoustics of the violin and viola.

LISA-7 has a library of isotropic and anisotropic elements which can be used for static problems of elastic deformation. However, dynamic analysis is limited to isotropic materials. This includes the important function of determining the normal modes of vibration, both their frequencies and displacement fields. Wood, being fibrous, is orthotropic: that is, its elastic properties are different in the three principal directions – longitudinal, radial and circumferential – in which the tree grows. Even thin plywood, with three plies, is stiffer along the surface grain than across it. In order to make at least some progress towards modelling the normal modes of wood and plywood using LISA, the question arises: 'Can some arrangement of isotropic component elements be found which will model the dynamics of orthotropic materials in LISA with sufficient accuracy?'.

LISA takes as data three mechanical properties of an isotropic material: Young's modulus E, Poisson's ratio ν, and the density ρ. Intuitively, we might expect that placing stiff fibres of isotropic material along the grain direction in a weaker matrix would give E along the grain larger than E across the grain. This has been the starting point for my search, though I believe models like this are used for carbon fibre and other layered composites. Since 3-ply plywood is of uniform thickness, about 3·5 mm, I judged it appropriate to model the vibration of plywood plates, starting with a square and graduating via rectangles to more irregular profiles. Before that, however, I have made comparisons for a square rolled aluminium sheet, aluminium being almost isotropic. The FEA-experimental agreement for aluminium defines a standard of modelling against which any model approximating orthotropic behaviour can be compared.

In the course of the study I accumulated experimental results, being frequency spectra and photographs of the vibrational pattern at each resonant frequency. These now constitute a database against which other theoretical and finite element models might be assessed. Note, however, that amplitudes of vibration at the antinodes have not been measured.

2 Experimental determination of normal modes

The resonant normal modes of vibration of an elastic structure are crucial to understanding the dynamic response under prescribed driving conditions because, at least for small amplitude vibrations, the response can be expressed as a sum over normal modes, weighted to match the boundary and driving conditions. Each normal mode is characterised by a) its frequency and b) its pattern of vibrational amplitude over the plate's surface. For the flat plates examined in this study the resonant frequencies can be determined by time spectrum analysis of tap sounds, which are the waveforms recorded through a microphone when the plate is tapped with a knuckle at various positions over its surface. These frequencies should coincide with resonances when the plate is excited by a steady sinusoidal driving pressure wave from, say, a loudspeaker. Resonance is manifest in the classic Chladni figure experiment[1] in which particles of dust are sprinkled over the plate, placed horizontally over the loudspeaker. Under the driving waveform the particles bounce around on the plate until most have settled in regions of nominally zero vertical velocity. As the frequency is varied, resonance can be judged from how vigorously the particles bounce about and from the crispness of the Chladni figure.

Resonances depend strongly not only on the mechanical properties of the plate but also on the way it is held – the boundary conditions. For a rectangular plate the most easy case to treat by analytical elasticity theory is that in which all four edges are simply supported. At a simply supported edge of a horizontal plate the vertical component of displacement is zero, but the plate is free to tilt locally, as if hinged. There are then no moments on the edge, so the plate remains locally flat at the edge, meaning that the second derivative of displacement there is also zero. Whilst the simply supported boundary condition is easy to realise in the static two-dimensional case of a narrow beam between supports (just rest the beam on straight parallel supports), it is experimentally perhaps the most difficult set of conditions to realise for a vibrating plate. It would involve clamping all four edges between horizontal rollers running precisely along the edge. In contrast, the simplest case to achieve experimentally is a free plate, resting on three or four very soft, spongy supports just above the exciting loud speaker. Unfortunately this is perhaps the most difficult case for mathematical elasticity to model, and research papers are still being written on the topic. Nevertheless it can in principle be modelling in LISA by having the plate free of all constraints. For this reason my experimental studies have been on free rectangular plates.

Figures 1 to 4 illustrate these two complementary techniques of measuring normal modes. Figure 1 is a tap waveform from a plywood rectangle detected on a recording quality capacitance microphone and captured using the Goldwave digital software. It shows a pattern of beats in the train of the impulse around the frequency of 217 Hz, as measured by counting cycles. The rectangle was Far Eastern plywood, 3·6 mm thick, 262 mm along the surface grain direction and 370 mm across. Figure 2 is the Fourier spectrum of this tap sound as produced by the WaveSpectra software. The cursor is set on the small peak at 218 Hz, but two larger peaks can be seen at 207 Hz and 230 Hz. These account for the pattern of beats. Other peaks can be distinguished at 16, 65, 110, 268, 283, 336, 357, 442, 525 and 565 Hz. The error in placing the cursor is about ±2 Hz. The 16 Hz peak is probably spurious. From analysis of six tap sounds made by knocking at different positions on the rectangle, a fairly consistent list of significant frequencies becomes clear. These are:

$$64,\ 101,\ 176,\ 207\ (\textit{largest}),\ 231,\ 266,\ 333,\ 441,\ 562,\ 603,\ 629\ \text{Hz}. \tag{1}$$

[1] Named after the central European physicist Ernst Chladni, 1756–1827.

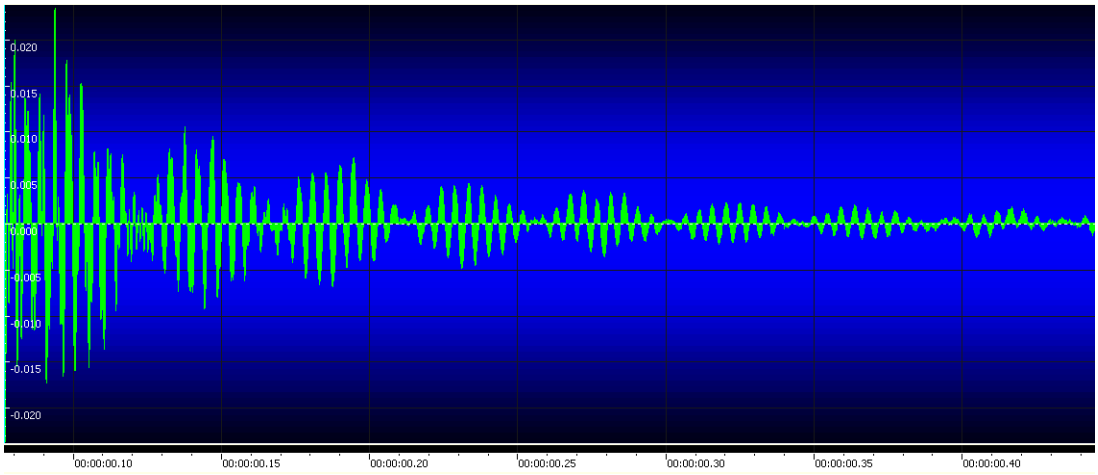

Figure 1: Waveform of tap sound from free plywood rectangle 262mm along grain × 370mm across.

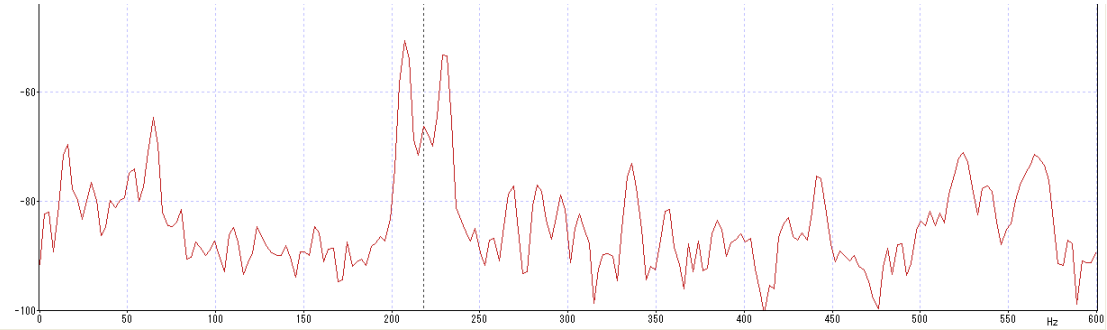

Figure 2: Frequency spectrum of waveform in Figure 1.

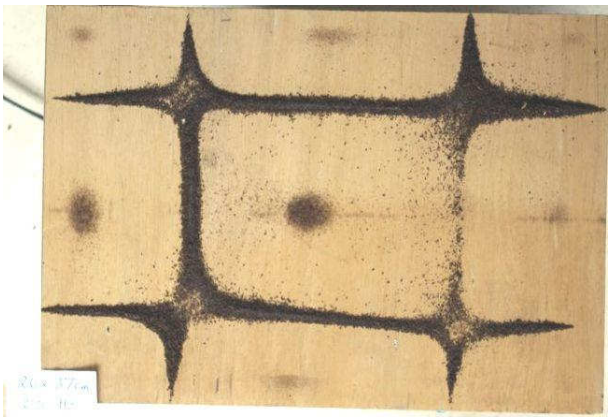

Figure 3: 270 Hz

Figure 4: 562 Hz

Chladni figures were obtained by laying the plate horizontally on top of an upwards-directed loudspeaker, the plate being supported 2 or 3 mm above the speaker on three or four crumbs of upholstery foam. Dust was sprinkled over the plate – a mixture of dry soil and fine peat. A woofer speaker was used up to about 200 Hz and a smaller speaker above that, up to about 1700 Hz. A digital tone generator delivered a continuous sine wave into the loudspeaker and the volume was adjusted until the dust particles started to dance. The soil collects mainly at positions of zero or

small vertical velocity (that is, velocity transverse to the plate). These are the node lines. Smaller, less distinct islands of dust sometimes remain at the antinodes because the plate surface locally is exactly horizontal, meaning that there is no component of force on the particles parallel to the plate. The position of the plate over the speaker is adjusted such that excitation is at an antinode. Where two or more modes have very similar frequencies, it is usually a delicate operation of adjusting the loudspeaker to obtain the Chladni figure for only one mode. A Chladni figure would develop in about a minute, as illustrated in Figures 3 and 4 for the plywood plate. The surface grain runs vertically in these pictures. The frequency was set initially at a dominant frequency in the tap-tone spectra, but sometimes adjusted by a few hertz by hand to obtain the most vigorous vibration and sharpest pattern.

3 Comparison for an isotropic plate

This section addresses the question of how close an agreement can be expected between finite element modelling and experimental measurement for the simplest case of an isotropic material, for which LISA does offer modal analysis. We should hope for quite good agreement for the rolled aluminium plate. This was $1{\cdot}0$ mm thick as measured with a screw micrometer, and almost square at $302{\cdot}9$ mm along the rolling direction by $301{\cdot}8$ mm across.

From the spectra of tap tones I obtained the dominant frequencies, and then drove the plate at a selection of these frequencies with the loudspeaker as described above. Figures 5 and 6 show predicted and experimental Chladni nodal patterns for eight resonances. The curving of node lines near what would otherwise be points of intersection can be attributed to mechanical damping. Damping broadens the resonance, including small components of the modes higher and lower in frequency. A few other modes gave Chladni figures as clear as those in Figures 5 and 6, including the ring mode at 64 Hz. However others were difficult to distinguish. Because the plate is almost square, some of the modes are almost degenerate. LISA predicts them as distinct in pattern (they are related by symmetry such as exchanging x and y axes) but occurring at the same frequency. In reality these modes are superimposed and the balance between them depends sensitively on how the plates are driven from the loudspeaker. Therefore, where resonant frequencies are close together, good agreement with experiment cannot be expected. Agreement is also poor at low frequencies where a general shaking of the plate occurs but the Chladni figure is indistinct.

LISA calculates both modal frequencies and modal patterns of transverse displacement. The contours of zero displacement correspond to Chladni figures. Hence, where experimental patterns are clear, they could be matched unambiguously with the model. In the LISA modelling the plate was represented by a 36×36 array of square quad8 shell elements which can be seen in the top right LISA image in Figure 5. They had these properties: thickness $1{\cdot}0$ mm, Young's modulus $70{\cdot}3$ GPa, Poisson's ratio $0{\cdot}345$, density 2720 kg m^{-3}. The density was chosen so that the weight of the plate was 248 g, as measured. This is close to published densities of aluminium. Young's modulus and Poisson's ratio were taken from published tables.

Table 1 compares all the predicted and experimental frequencies. Overall the agreement is highly satisfactory. Note that because the plate is free, the only constraint coming from its own weight, no constraints are added to the LISA model[2]. A consequence of this is that the six lowest

[2]The finite element matrix is singular when the plate is completely free of constraints and some FEA codes will not tolerate this condition. They require, for example, that supporting soft springs be modelled too. LISA does tolerate no constraints, in which case the first six modes correspond to rigid body translations and rotations. For some other calculations I have added 3 constraints on displacement, in which case the first mode with deformation is mode 4.

modes describe bodily translations and rotations of the plate without distortion. That is why the lowest vibrational mode number is 7.

mode	LISA (Hz)	Expt (Hz)	mode	LISA (Hz)	Expt (Hz)
7	36		21	357	351
8	52	50	22	359	361
9	67	64	23	413	411
10	93	101	24	437	431
11	93	98	25	459	452
12	166	167	26	543	537
13	167		27	547	
14	170	188	28	556	551
15	185	190	29	586	582
16	210	214	30	587	
17	283	277	31	589	592
18	284		32	664	
19	319	314	33	667	658
20	336	336	34	768	754

Table 1: Comparison of normal mode frequencies (Hz) predicted by LISA and measured experimentally for a 302 mm square, 1 mm thick flat aluminium plate.

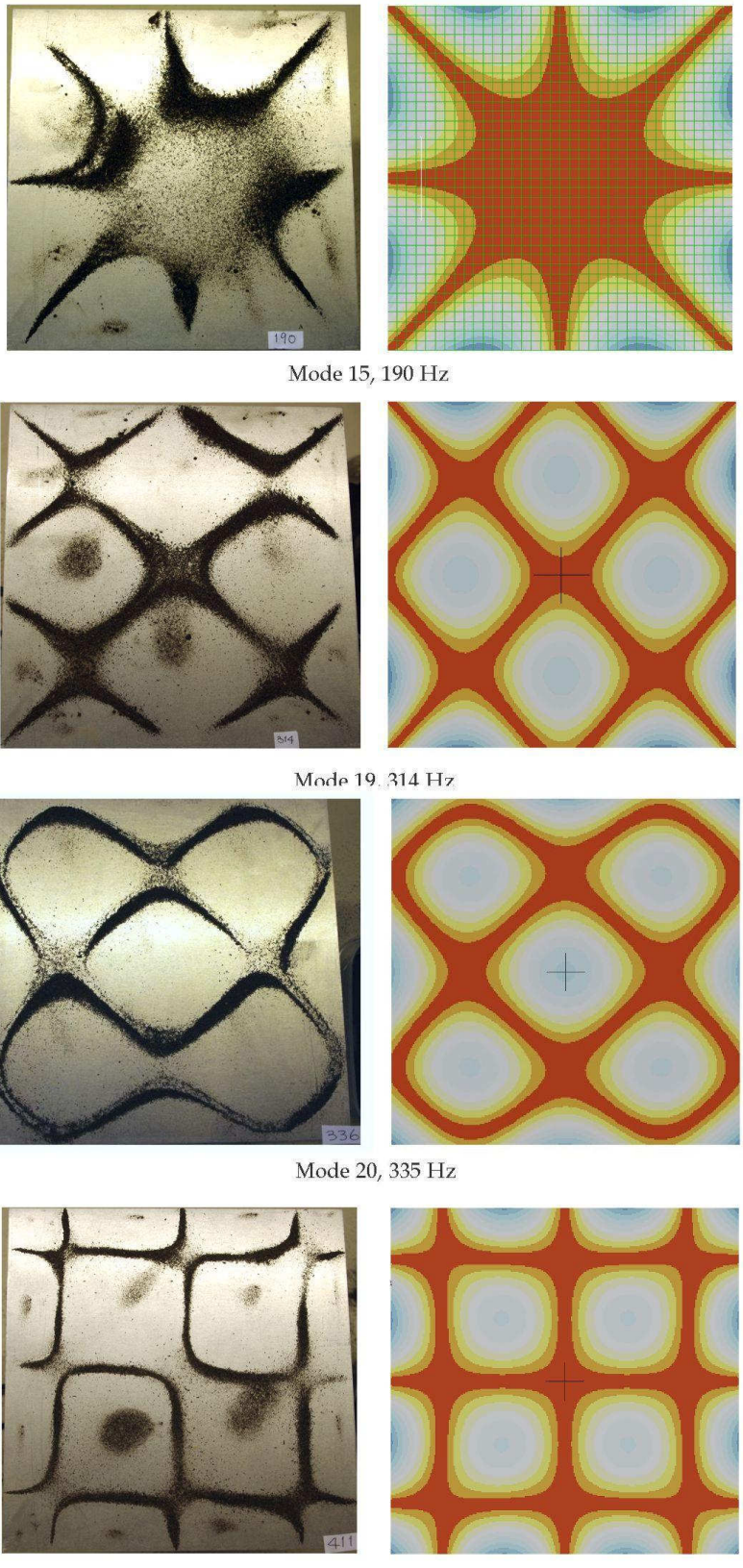

Figure 5: LISA depictions of contours of transverse displacement in four normal modes of aluminium plate 302 mm square, compared with experimental Chladni figures. The top right LISA image shows the grid of finite elements.

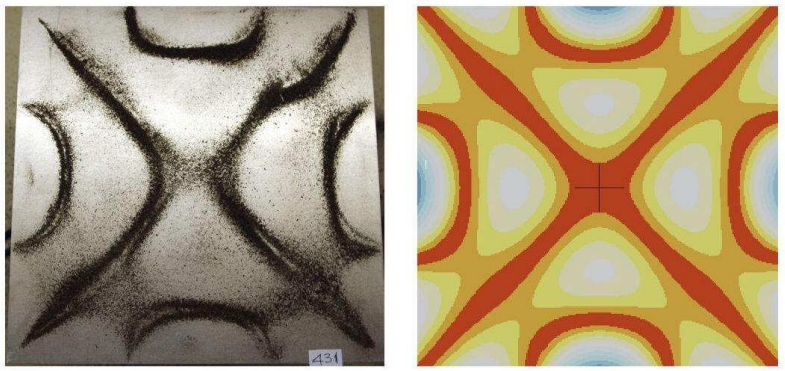

Mode 24, 431 Hz

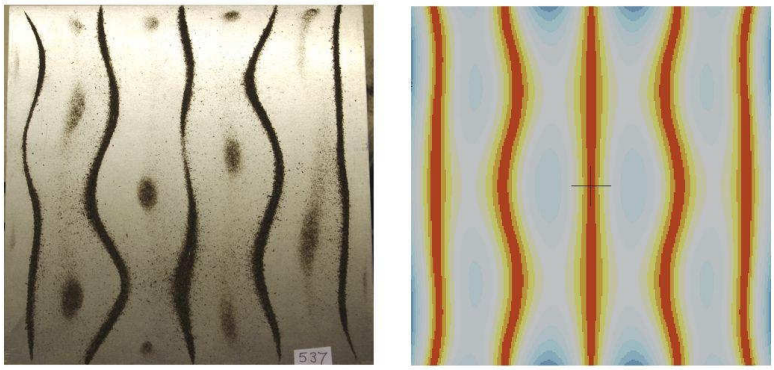

Mode 26, 537 Hz

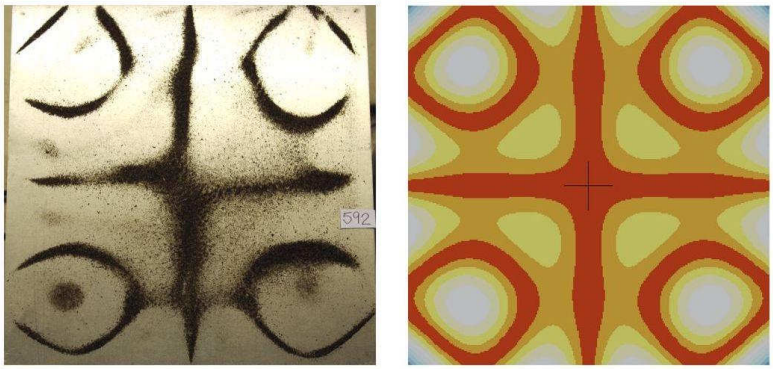

Mode 31, 592 Hz

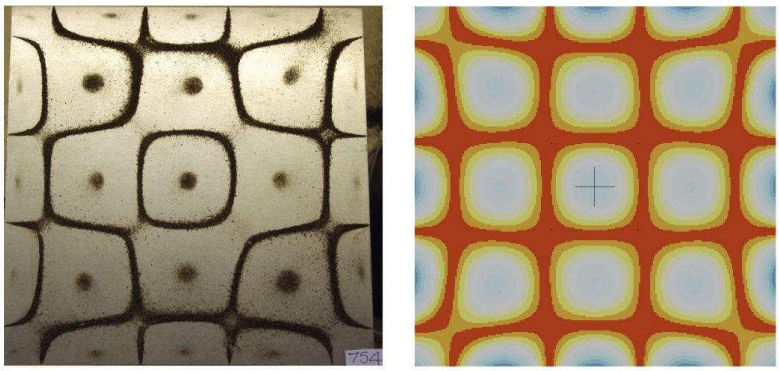

Mode 34, 754 Hz

Figure 6: LISA depictions of contours of transverse displacement in four higher frequency modes of square aluminium plate compared with experimental Chladni figures.

4 Insights from theory

Though there is no closed form formula for the resonant frequencies of a free plate, we have a guide to their probable dependence on elastic constants and plate dimensions from the corresponding formulae for a simple supported beam and simply supported plate. The classical equation of motion for small amplitude transverse vibrations of a beam is

$$EI\frac{\partial^4 u}{\partial x^4} + \frac{M}{L}\frac{\partial^2 u}{\partial t^2} = 0 \tag{2}$$

where u is the displacement, x the distance along the beam, I is the moment of cross-sectional area, which equals $bh^3/12$ for a rectangular section. M is its mass, L its length, h the thickness and b the breadth. The general solution is the sum of eight terms $(c_1 \cos\alpha x + c_2 \sin\alpha x + c_3 \cosh\alpha x + c_4 \sinh\alpha x)\cos\omega t + (c_5 \cos\alpha x + c_6 \sin\alpha x + c_7 \cosh\alpha x + c_8 \sinh\alpha x)\sin\omega t$ where the c_j are constants fitted to the boundary conditions and

$$\frac{M}{EIL} = \frac{\alpha^4}{\omega^2} \quad \text{giving} \quad f = \frac{\alpha^2}{2\pi}\sqrt{\frac{EIL}{M}}, \tag{3}$$

f being the frequency in Hz. α has dimensions 1/length and can be taken to be a multiple of $1/L$. The resonant frequencies therefore scale with h, L, E and density ρ according to

$$f_j = K_j \frac{h}{L^2}\sqrt{\frac{E}{\rho}} \tag{4}$$

where the K_j are constants depending on boundary conditions and order j of the mode. Note that f_j do not depend on the width b of the beam. Eq 4 expresses the common experience that a thicker, stiffer plate has a higher tap sound than a thinner, limper one.

The dependence on L^2 rather than L is also surprising, since for a stretched string frequency is inversely proportional to length [3]. However, whilst a string satisfies a second order pde, a beam satisfies a fourth. The capacity of a beam to sustain compressive and shearing forces requires the non-oscillatory terms in $\cosh\alpha x$ and $\sinh\alpha x$. These are not present in the formula for displacement of a string.

The formulae above for a beam depend only on the one length dimension, x. When the beam is widened to become a rectangular plate, three main changes occur:

1. equivalent beam-like modes occur for the y dimension,
2. modes depending on both x and y occur, some of which describe twisting of the plate,
3. plane strain conditions apply and E is replaced by $E/(1-\nu^2)$. We write $1-\nu^2 = \lambda$.

Nevertheless, the frequencies scale with h, L, E and ρ essentially as Eq 4. The equation of motion for an isotropic plate is a generalisation of Eq 2:

$$\frac{EI}{\lambda}\nabla^4 u + \frac{M}{L}\frac{\partial^2 u}{\partial t^2} = 0 \tag{5a}$$

[3] Unlike a beam which is intrinsically stiff, stiffness in a string is due solely to the applied tension. The fundamental frequency of a string, length L, stretched at tension T between fixed end grips is $f = \frac{1}{2L}\sqrt{\frac{T}{\rho'}}$ where ρ' is the mass per unit length. To make this appear closer to the beam formula let the cross sectional dimensions of the string be b and h so that the total mass is $m = \rho' L = \rho L h b$. Then the stress in the string is $\sigma = T/hb$ and $f = \frac{1}{2L}\sqrt{\frac{\sigma}{\rho}}$. Young's modulus E has the dimension of stress.

where the biharmonic operator is

$$\nabla^4 u \;\equiv\; \frac{\partial^4 u}{\partial x^4} + 2\frac{\partial^4 u}{\partial x^2\,\partial y^2} + \frac{\partial^4 u}{\partial y^4}.$$

The literature on this subject introduces $D = Eh^3/(12\lambda) = EI/(b\lambda)$, b being the breadth of the beam/plate. The equation of motion, as first set out by Love in 1927, then becomes

$$D\left(\frac{\partial^4 u}{\partial x^4} + 2\frac{\partial^4 u}{\partial x^2\,\partial y^2} + \frac{\partial^4 u}{\partial y^4}\right) + \frac{M}{bL}\frac{\partial^2 u}{\partial t^2} \;=\; 0. \tag{5b}$$

Note that $M/(bL) = \rho h$, the mass per unit area.

There is a further generalisation to an orthotropic plate (see next section for fuller explanation of orthotropic). In a classic early paper on the vibration of rectangular plywood plates R. Hearmon[4] quotes the equation of motion

$$D_1\,\frac{\partial^4 u}{\partial x^4} + 2D_3\frac{\partial^4 u}{\partial x^2\,\partial y^2} + D_2\frac{\partial^4 u}{\partial y^4} + \frac{M}{bL}\frac{\partial^2 u}{\partial t^2} \;=\; 0 \tag{6}$$

$$\text{where}\quad D_1 = \frac{E_x h^3}{12\lambda},\quad D_2 = \frac{E_y h^3}{12\lambda},\quad D_3 = \frac{E_x \nu_{yx} h^3}{12\lambda} + \frac{G_{xy} h^3}{6}.$$

E_x = Young's modulus in bending in the x direction,
E_y = Young's modulus in bending in the y direction,
ν_{yx} = contraction in x direction for unit extension in y when in tension along y direction,
$\lambda = 1 - \nu_{xy}\nu_{yx} \approx 0\cdot 99$ for wood and plywood,
G_{xy} = in-plane rigidity modulus for shear stresses in the x and y directions.

Hearmon also quotes the resonant frequencies of a specially orthotropic plate (i.e. one in which the grain is aligned with the edges of the rectangle) with four simply supported edges as

$$f_{m,n} \;=\; \frac{\pi}{2}\sqrt{\frac{1}{\rho h}}\sqrt{\frac{m^4}{a^4}D_1 + 2\frac{m^2 n^2}{a^2 b^2}D_3 + \frac{n^4}{b^4}D_2} \tag{7}$$

where a and b are the lengths of the plate parallel to the x and y axes respectively, and m and n are integers which index the nodes. The fundamental is at $m = n = 1$. Substituting and dropping some suffices,

$$f_{m,n} \;=\; \frac{\pi}{4\sqrt{3}}\frac{h}{\sqrt{\rho\lambda}}\sqrt{\frac{m^4}{a^4}E_x + 2\frac{m^2 n^2}{a^2 b^2}(E_x\nu + 2G)\lambda + \frac{n^4}{b^4}E_y} \tag{8}$$

This is an important expression for the resonant frequencies for a simply supported plywood plate. Observe that, as for the beam, resonant frequencies are directly proportional to thickness, h.

Resonance frequencies for a simple supported isotropic plate can be recovered from Eq 8. $G_{xy} \equiv G$ is then related to Young's modulus and a single Poisson's ratio ν by

$$G \;=\; \frac{E}{2+2\nu} \;=\; 0\cdot 384E \text{ for } \nu = 0\cdot 3, \tag{9}$$

[4] R F S Hearmon 1946 Proc. Phys. Soc. **58** 78

$0{\cdot}3$ being typical of many materials. The limits on ν for an isotropic material are $-1 < \nu < 0 \cdot 5$. Setting $E_x = E_y = E$ we have

$$f_{m,n} \;=\; \frac{\pi}{4\sqrt{3}}\,\frac{h}{ab}\sqrt{\frac{E}{\lambda\rho}}\sqrt{\frac{b^2}{a^2}m^4 + 2m^2n^2 + \frac{a^2}{b^2}n^4} \tag{10}$$

where the factor ab = plate area has been taken to leave the argument of the long square root as a dimensionless number. (The Poisson's ratio expression in Eq 8 is $\left(\nu + \frac{\lambda}{\nu+1}\right)$ but this evaluates to 1.) There is a similarity to Eq 4 for a beam and the beam formula can be recovered by the following limiting process. Recall that the plate is simply supported on all four edges but the beam is simply supported only at $x = 0$ and $x = L$. The two free edges of the beam can be approximated by taking the two corresponding sides of the plate to infinity. Thus let $a = L$ and $b \to \infty$. Only the term in m^2 inside the root contributes significantly and we are left with

$$f_1 \;\approx\; \frac{\pi}{4\sqrt{3}}\,\frac{h}{L^2}\sqrt{\frac{E}{\rho}}.$$

Compare this with Eq 4.

5 Experimental characterisation of a plywood plate

5.1 Elastic constants of plywood

As already noted, plywood is orthotropic, having three orthogonal two-fold axes of rotational symmetry – along the surface grain, across the grain, and through the thickness. It therefore has 9 independent elastic constants. The compliance tensor $\mathbf{S}_{ij}$, when written as a matrix with the standard reduced subscripts $11 \to 1$, $22 \to 2$, $33 \to 3$, 23 and $32 \to 4$, $13/31 \to 5$, $12/21 \to 6$, relates stress to strain by

$$\begin{pmatrix}\epsilon_1\\ \epsilon_2\\ \epsilon_3\\ \epsilon_4\\ \epsilon_5\\ \epsilon_6\end{pmatrix} = \begin{pmatrix} \frac{1}{E_1} & \frac{-\nu_{21}}{E_2} & \frac{-\nu_{31}}{E_3} & 0 & 0 & 0\\ \frac{-\nu_{12}}{E_1} & \frac{1}{E_2} & \frac{-\nu_{32}}{E_3} & 0 & 0 & 0\\ \frac{-\nu_{13}}{E_1} & \frac{-\nu_{23}}{E_2} & \frac{1}{E_3} & 0 & 0 & 0\\ 0 & 0 & 0 & \frac{1}{G_4} & 0 & 0\\ 0 & 0 & 0 & 0 & \frac{1}{G_5} & 0\\ 0 & 0 & 0 & 0 & 0 & \frac{1}{G_6} \end{pmatrix}\begin{pmatrix}\sigma_1\\ \sigma_2\\ \sigma_3\\ \sigma_4\\ \sigma_5\\ \sigma_6\end{pmatrix} = \begin{pmatrix} \frac{1}{E_1}(\sigma_1 - \nu_{12}\sigma_2 - \nu_{13}\sigma_3)\\ -\frac{\nu_{12}\sigma_1}{E_1} + \frac{\sigma_2}{E_2} - \frac{\nu_{23}\sigma_3}{E_2}\\ -\frac{\nu_{13}\sigma_1}{E_1} - \frac{\nu_{23}\sigma_2}{E_2} + \frac{\sigma_3}{E_3}\\ \sigma_4/G_4\\ \sigma_5/G_5\\ \sigma_6/G_6 \end{pmatrix}$$

The matrix is symmetric so the 6 Poisson's ratios are related through three expressions of the form

$$\frac{\nu_{21}}{E_2} \;=\; \frac{\nu_{12}}{E_1}.$$

These relations have been used in evaluating the strain matrix on the right. Note that zeros in $\mathbf{S}_{ij}$ mean that tensile stresses do not produce shear distortions and shear stresses do not produce extensions.

For a model of wood to fit experiment, measurement must be made of the relevant elastic constants as well as the modal frequencies and Chladni patterns. The material used is known as Far Eastern plywood. Its surface layers are birch and the middle meranti. It is not easy to measure all 9 elastic constants by simple techniques, but 4 can be found. These are Young's modulus in the two orthogonal directions in the plane of the plywood, and two shear moduli by twisting a strip oriented

either along or across the grain. Young's modulus was measured by bending a strip typically 2 or 3 cm wide, 30 or 40 cm long, as a simply supported beam under a central load. E is given by

$$E = \frac{1}{4b}\left(\frac{Wg}{d}\right)\left(\frac{L}{h}\right)^3 \qquad \text{SI units, N/m}^2 \tag{11}$$

where W is the load in kilograms, g the gravitational acceleration, d the maximum (central) displacement in metres,, L the length of beam between its supports, h its thickness and b its breadth. One shortcoming of this method for E is that the result depends sensitively on the thickness h. This was measured using both a micrometer and dial gauge and found to vary between $3{\cdot}44$ mm and $3{\cdot}80$ mm over the plate, indicating that the original plywood sheet was slightly tapered. Values used in calculating E are the means of about half a dozen measurements on each specimen.

The shear (rigidity) modulus was measured dynamically by making a strip of ply into the vertical twisting bar of a torsion pendulum. A metre long beam of wood was screwed centrally onto one end of the ply strip to form an inverted T shape, and the upper end of the strip specimen gripped in a vice. The beam was turned through about 10^o without lateral displacement and released, and the oscillations timed. For a static rotation, the angle of twist, θ, is related to the torque T (Nm), length L of the strip and rigidity modulus G by

$$\theta = \frac{TL}{JG} \tag{12}$$

where J is a shape factor related to the moment of cross-section of the strip:

$$J = bh^3\left[\frac{1}{3} - \frac{21}{100}\left(\frac{h}{b}\right) + \frac{7}{400}\left(\frac{h}{b}\right)^5\right].$$

G is inversely proportional to the square of period of oscillation t:

$$G = \frac{4\pi^2}{t^2}\,\frac{LI}{J} \tag{13}$$

where I is the moment of inertial of the heavy beam about the axis of rotation. In this measurement the value of G relates to shear of the strip in the through-thickness direction. With the surface grain along the strip specimen and the torque forces applied in the through thickness direction 3, $G_{\parallel} = G_{13} = G_5$ is measured. Similarly with the surface grain across the specimen $G_{\perp} = G_{23} = G_4$ is measured.

The values obtained from several specimens and/or series of measurements using the above methods are listed in Table 2. The measurement methods used will be simulated using LISA to promote a close match between the FEA model and reality. The ratio $E_{\parallel}/E_{\perp} = 2 \cdot 95$.

5.2 Experimental determination of normal modes of 262 mm plywood square

The techniques of §2 were applied to a 262 mm square of the 3-plywood. Figure 7 shows two frequency spectra from tapping the square. Though similar, they differ in detail because holding the plate in different places, and tapping at different places, excite modes in different proportions. Damping within the wood causes broadening and hence some overlapping of resonant peaks. As a result a wholly consistent sets of frequencies cannot be determined from the spectra, though about a dozen frequencies appear in most spectra.

		SI units
total thickness	$3 \cdot 4$ to $3 \cdot 8$ mm	$0 \cdot 0036$ m
birch veneers, typical	$0 \cdot 53$ & $1 \cdot 00$ mm	
central meranti layer	$2 \cdot 07$ mm	
density	$0 \cdot 68$ g/cc	680 kg/m^3
Young's modulus, grain parallel to strip	$E_{\|} = E_1$	$10 \cdot 2$ GPa
Young's modulus, grain across strip	$E_{\perp} = E_2$	$3 \cdot 46$ GPa
Shear modulus, grain parallel to strip	$G_{\|} = G_5$	$0 \cdot 46$ GPa
Shear modulus, grain across strip	$G_{\perp} = G_4$	$0 \cdot 55$ GPa

Table 2: Dimensions and material properties of Far Eastern plywood as measured on strip specimens. 1 GPa = 10^9 N/m^2.

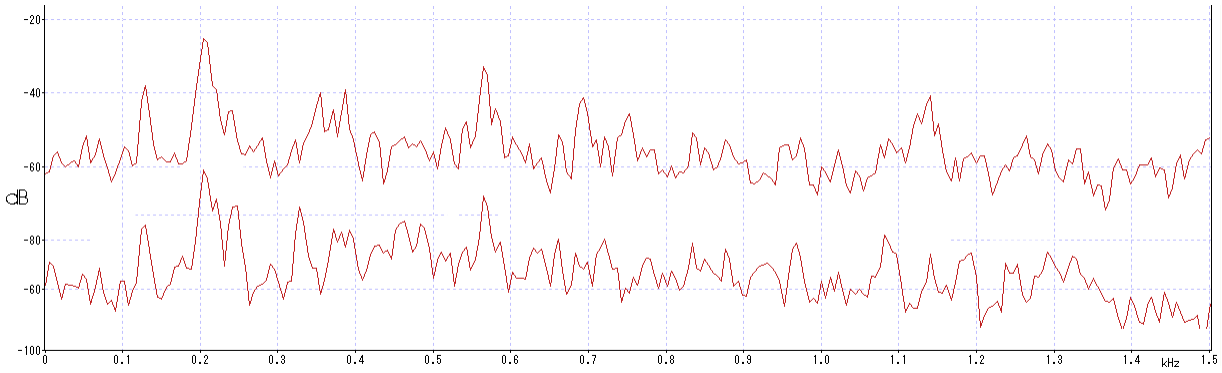

Figure 7: Frequency spectra of two tap sounds from the 262mm plywood square. Frequency range 0 to 1500 Hz.

The resonance peaks in the spectra guided the search for the corresponding Chladni figures. The loudspeakers available were useful over the range from about 40 Hz to 1800 Hz. Considerable pains were taken to isolate the Chaldni figure of only single modes in frequency ranges where two or more modes have much the same frequency, as occurs over the range 1070 to 1150 Hz. Figure 8 presents photographs of all the Chaldni resonances determined. The surface grain is vertical in all these photographs. In this array presentation rows are labelled m and the columns n, where the mode $m - n$ means that there are m node lines in the x direction and n along the y: that is, there are m dark, roughly vertical node lines, parallel to the grain, and n roughly horizontal lines (across the grain). Table 3 lists the best estimates of the corresponding frequencies. The modes 0-4, 1-4, and 5-0 were particularly difficult to disentangle so the errors for these could be as large as 20 Hz. Otherwise uncertainty is about 4 Hz. (Mode 6-1 is identified with the resonance at 1736 Hz, but this was the only mode not confirmed by Chladni figure.)

The two graphs in Figure 9 display the dependence of resonant frequency on the mode numbers m and n. The upper graph corresponds to reading Table 3 by the column (m varies while n is constant on each curve), and the lower panel by reading in rows. Over this range of frequencies each curve is roughly parabolic. Within the approximation of terms up to degree 2, the frequencies f are roughly approximated by the doubly quadratic expression

$$f \approx 79 \cdot 2 - 97 \cdot 4m - 109 \cdot 3n + 61 \cdot 9m^2 + 39 \cdot 5mn + 90 \cdot 0n^2 - 3 \cdot 8m^2n - 4 \cdot 4mn^2 - 1 \cdot 2m^2n^2$$

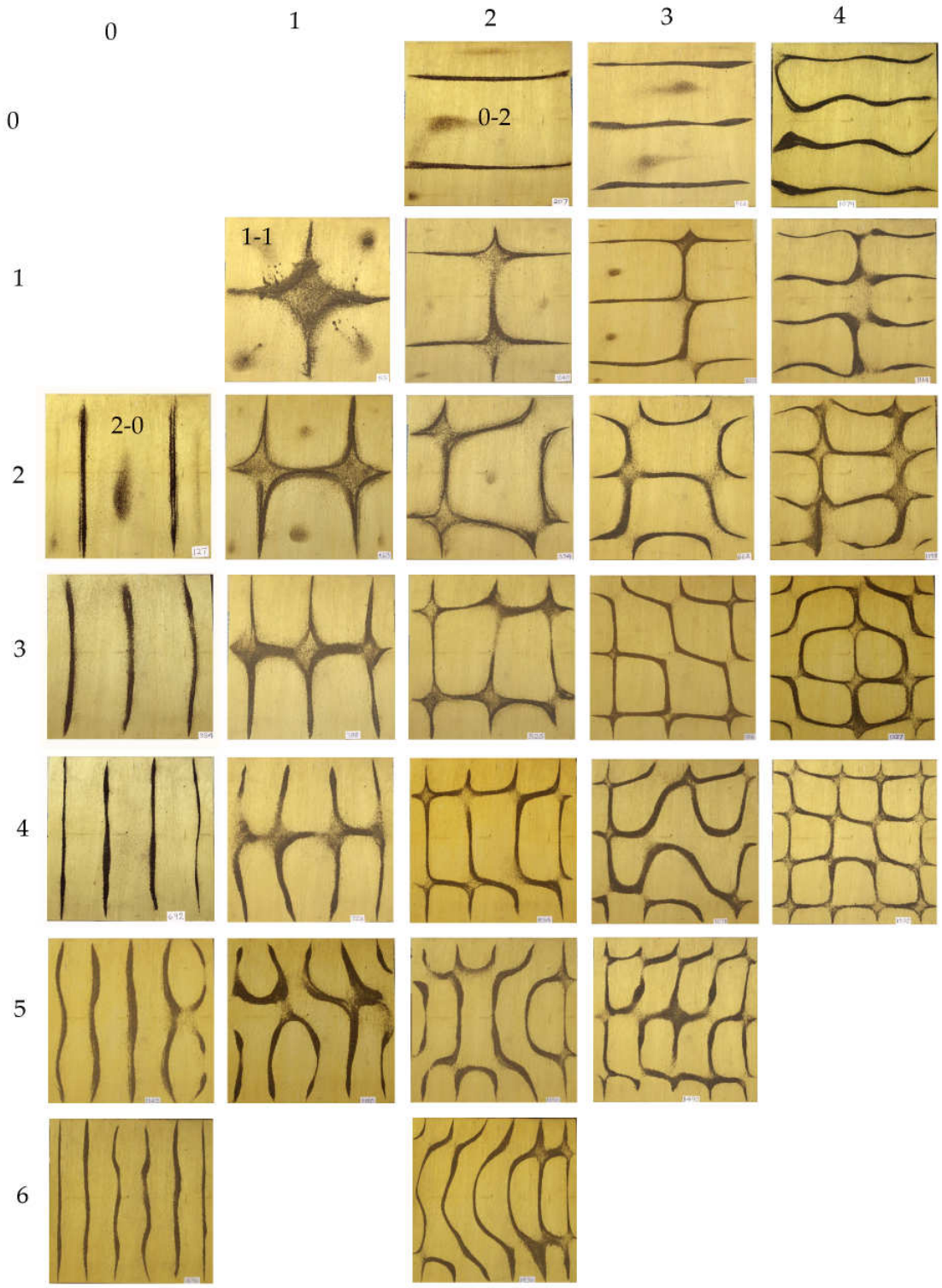

Figure 8: Photographs of experimental Chladni figures for a 262 mm square plywood plate. The surface wood grain is vertical on the page, parallel to the y axis.

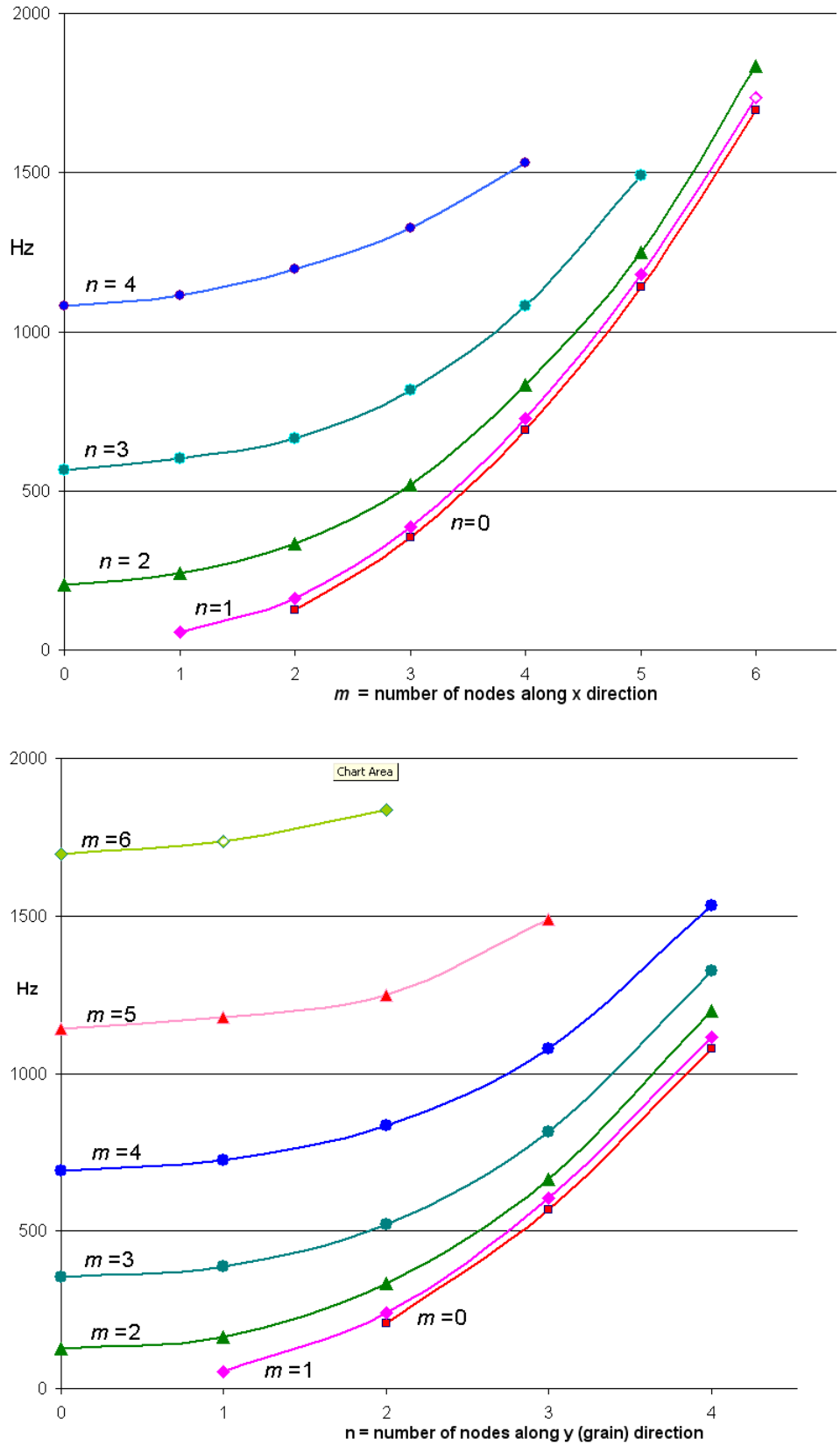

Figure 9: Variation in frequency of mode families with increasing number of node lines in x direction (lines parallel to the grain).

x	y				
	0	1	2	3	4
0			206	566	1080
1		55	240	603	1114
2	127	163	334	663	1198
3	354	388	520	816	1327
4	692	726	834	1080	1532
5	1142	1180	1250	1490	
6	1696	*1736*	1836		

Table 3: Experimentally determined frequencies of modes identified in Figure 7.

which can be neatly written in matrix form as

$$(f) \approx \begin{pmatrix} 1 & m & m^2 \end{pmatrix} \begin{pmatrix} 79\cdot 2 & -109\cdot 3 & 90\cdot 0 \\ -97\cdot 4 & 39\cdot 5 & -4\cdot 4 \\ 61\cdot 9 & -3\cdot 8 & -1\cdot 2 \end{pmatrix} \begin{pmatrix} 1 \\ n \\ n^2 \end{pmatrix} .$$

This is an empirical fit; clearly other quadratic and higher polynomials could be fitted to the data.

What is perhaps more interesting is to see where these frequencies lie on a piano keyboard. Figure 10 shows a grand piano keyboard with coloured spots at the frequencies of the mode families for m varying, n fixed. $n = 0$ is red, $n = 1$ is purple, then green, turquoise and blue. Observe how the low resonant frequencies are sparse but the higher ones bunch together. This is a consequence of the logarithmic nature of perceived pitch. I venture at this juncture to conjecture on the consequences of this distribution of modal frequencies for a stringed musical instrument, such as a 'cello. A good quality of sound probably requires a fairly even spacing of resonances across the compass of the instrument. Figure 10 shows a very uneven spacing, with few in the lowest register and significant bunching about two octaves about middle C. This bunching is partly a consequence of the mode degeneracy occasioned by the square symmetry of the plate. Asymmetry is more likely to spread the resonances evenly. An instrument with these resonances could be weak and uneven in the lowest and possibly harsh in the higher.

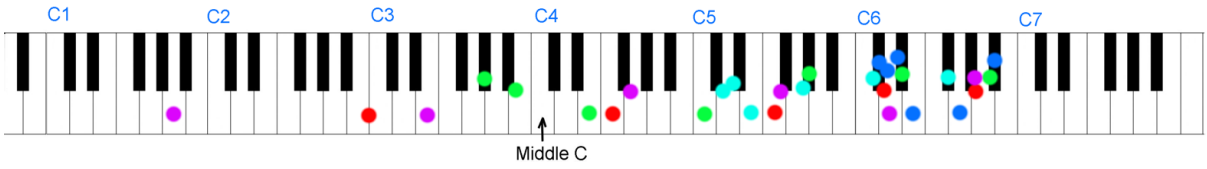

Figure 10: A piano keyboard with coloured spots marking the modal frequencies in Table 3.

6 Development of a 2-D shell model of orthotropic material

6.1 2-D quasi-orthotropic shell finite elements

This section describes attempts to model the vibration of thin plates of uniform thickness in LISA using isotropic two dimensional quadratic 'quad8' shell elements. The first stage is to produce Young's moduli $E_{||}$, $E_{\perp}$ matching experiment.

The virtual quasi-orthotropic material will be made from parallel strips of stiff (A) and compliant (B) isotropic materials. The starting point for analysis is the arithmetic of combining springs in parallel and in series. This is because along the direction of the strips they act as elastic strips in parallel whilst across the strips they are in series. By considering the forces and displacements of N springs of equal length in parallel it is straightforward to show that the effective spring constant is

$$E_{parallel} = \frac{n_1}{N}E_1 + \frac{n_2}{N}E_2 + \dots \qquad (14a)$$

where n_j of the springs have stiffness E_j. Transferring this to strips of elastic material in parallel, the effective Young's modulus is the sum of Young's moduli for the component materials weighted by their volume fraction p. Similarly, the effective stiffness of N springs in series is the weighted sum of reciprocals

$$\frac{1}{E_{series}} = \frac{n_1}{N}\frac{1}{E_1} + \frac{n_2}{N}\frac{1}{E_2} + \dots \ . \qquad (14b)$$

Choose materials A and B to have $E_A > E_{||}$ and $E_B < E_{\perp}$ and solve the two simultaneous equations

$$E_{||} = 10 \cdot 2 = pE_A + (1-p)E_B, \qquad \frac{1}{E_{\perp}} = \frac{1}{3 \cdot 46} = \frac{p}{E_A} + \frac{1-p}{E_B}. \qquad (15)$$

The graphs in Figure 11 illustrate these functions and show that the largest separation of the curves is near $p = 2/3$. In forming the finite elements in LISA it may be convenient to have their widths a simple multiple of some suitable unit, so I will choose $p = 2/3$ exactly. This then requires that $E_A = 14 \cdot 615$ GPa, $E_B = 1 \cdot 367$ GPa.

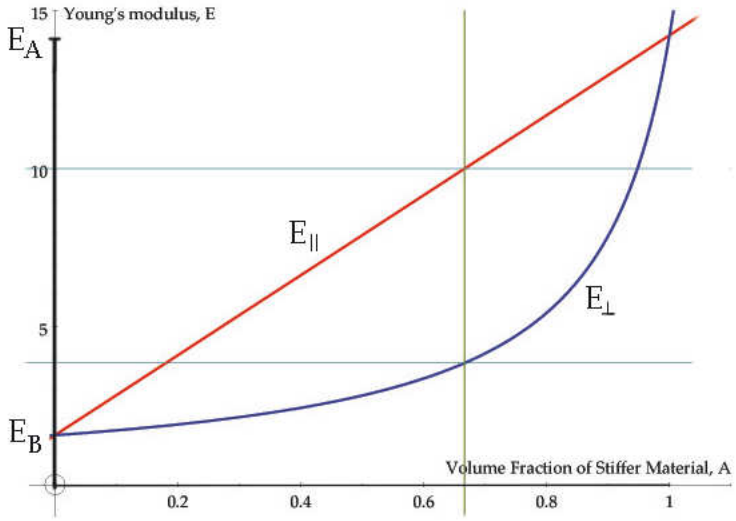

Figure 11: Effective Young's moduli $E_{||}$, $E_{\perp}$ as a function of volume fraction p of stiff material A in compliant material B. The vertical scale is in GPa.

Since LISA is being used to model the vibration of plates, LISA will also be used to check the values of $E_{||}$ and $E_{\perp}$ by modelling the static measurement methods of §5.1. Accordingly I constructed in LISA a model of a thin strip in bending with these parameters:

- 30 elements (10 ABA sets) wide in x direction, with materials in order ABAABA....AABA, by 30 elements long in y,
- an alternative, finer meshed model with 60 elements wide in x, forming 20 ABA units, by 60 elements long in y,
- $E_A = 14 \cdot 615$ GPa, $E_B = 1 \cdot 367$ GPa as above, with Poisson's ratio $0 \cdot 3$ in the first instance.
- length $L = 0 \cdot 5$ m, width $b = 0 \cdot 03$ metres, thickness $h = 0 \cdot 00352$ m,
- constraint on all nodes at $y = 0$ and at $y = 0 \cdot 5$ set to z displacement $= 0$,
- force of 1 newton applied in z direction at every node at central position, $y = 0 \cdot 25$, making the total force 61 N.

Three simulations were made with 2-D quad8 or quad9 shell elements in the above models:

1. bending to determine $E_{||}$ and $E_{\perp}$. These give $E_{||} = 10 \cdot 204$ GPa, $E_{\perp} = 3 \cdot 656$ GPa.
2. uniaxial stretching to determine $E_{||} = 10 \cdot 208$ and $E_{\perp} = 3 \cdot 64$ GPa,
3. twisting to determine $G_{||} = 1 \cdot 51$ and $G_{\perp} = 3.05$ GPa,

The agreement between the bending and stretching methods for the two Young's moduli is encouraging, as is the closeness of the simulated values to the required ones. However, the shear moduli are clearly far too large – between three and six times larger than the measured ones. This is not unexpected since, in this model of adjacent strips, Young's modulus in the through-thickness direction will equal that in the along-grain direction. In reality plywood is weak and compliant through its thickness since this direction corresponds with the radial direction of wood growth. At least LISA predicts that $G_{\perp} > G_{||}$ in agreement with experiment.

6.2 LISA 2D shell model compared with experiment

The predicted modal frequencies for this 2-D shell element quasi-orthotropic material for the 262 mm square plywood plate are listed in Table 4. The corresponding experimental values of Table 3 are reproduced in italics in the row below. At a glance we see that agreement is quite good for the $0-n$ and $m-0$ modes but poor in all other cases, as the predicted frequency exceed the actual typically by 20% to 40%.

LISA does predicted the general trend in frequency and does separate the corresponding pairs of modes $(0-2, 2-0)$, $(0-3, 3-0)$ etc. For an isotropic plate these would be at the same frequency. Table 5 shows the ratio of experimental frequencies of mode pairs $m-0$ to $0-n$. Using the relation that $f \propto \sqrt{E}$ in Eqs 4 and 10, the table has been artificially extended to zero frequency by taking the ratio of square roots of the Young's moduli. There is a steady trend to decreasing ratio with increasing frequency. However, Eq 8 would predict a constant value of $1 \cdot 717$. For all other modes the fact that the FEA frequency far exceeds the measured can be attributed to this 2-D model being too stiff in twisting, a fact already established by the twisting model for determining $G_{||}$ and $G_{\perp}$. There seems no point in finessing this 2-D model, say by adjusting E_A and E_B. Rather it seems

clear that closer agreement will require a more sophisticated quasi-orthotropic model in which E in the through thickness dimension can be adjusted independently to a much lower value.

The need to move to a more complicated 3D model is disappointing because 2D elements have significant advantages for thin-walled structures. Having fewer nodes, they produce smaller files, plus they have the through-thickness behaviour built into the elements. As with all numerical procedures, convergence to the correct solution usually requires a sufficient number of small elements, meaning very many nodes. LISA is a 32-bit computer program running under Microsoft Windows and so is limited to 2Gb of memory by the operating system no matter how large the physical memory. Therefore 3D models will inevitably be limited in size and hence fineness of mesh.

		n					
	m	0	1	2	3	4	5
FEA 2-D	0			208	570	1116	1854
Expt				*206*	*566*	*1080*	
	1		114	260	663	1204	1925
			55	*240*	*603*	*1114*	
	2	122	304	517	899	1436	2155
		127	*163*	*334*	*663*	*1198*	
	3	345	482	794	1214	1784	
		354	*388*	*520*	*816*	*1327*	
	4	671	806	1152	1620	2224	
		692	*726*	*834*	*1080*	*1532*	
	5	1108	1247	1596	2105		
		1142	*1180*	*1250*	*1490*		
	6	1659	1782	2145			
		1696	*1736*	*1836*			

Table 4: Comparison of resonant frequencies of a 262 mm square plywood plate as modelled by 2-D finite elements (LISA) and determined experimentally (italics). The finite elements are quasi-orthotropic 2-D shell using $E_A = 14 \cdot 615$ GPa, $E_B = 14 \cdot 367$ GPa, $\nu = 0 \cdot 3$.

Static	value	mode	Hz	ratio
$\sqrt{E_\perp}$	$1 \cdot 86$			$1 \cdot 717$
$\sqrt{E_\parallel}$	$3 \cdot 19$			
		2-0	127	$1 \cdot 622$
		0-2	206	
		3-0	354	$1 \cdot 600$
		0-3	566	
		4-0	692	$1 \cdot 560$
		0-4	1080	

Table 5: Ratios of experimental frequencies for modes with node lines parallel with one plate edge.

7 3-D solid model of orthotropic material

7.1 Basic 27-element building block

There are many ways in which the 2-material AB composite shell elements of §6 could be generalised to three dimensions with sufficient parameters to allow a fit to the measured elastic constants. Similar to the 2D case, the material will be built by translating and scaling a basic cuboidal block comprising an assemblage of isotropic hex20 finite elements. I have taken the view that this composite building block be symmetrical, or almost symmetrical, in the thickness dimension, just as the plywood itself is a sandwich of meranti between two sheets of birch. Unless there is such symmetry, I suspect that unrealistic bending or twisting of the modelling plate could occur. Accordingly, the building block has three layers with 9 elements in each. Moreover, the two outer layers will have the stiffening running parallel to the surface birch grain, whilst in the central layer it will run parallel with the grain of the meranti. I use two materials in each layer, requiring four materials, A, B, C, D, altogether. In addition, I have decided to keep all finite elements the same size within this building block. Finally, the material is to be as homogeneous as possible. This requires that adjacent elements be made of different materials as far as possible; they should not aggregate into extended clumps of elements of the same material when tessellated through the structure.

The design of building block is shown in Figure 12. The three diagrams in the top panel show the elements in each of the three layers through the thickness, whilst the bottom panel is a perspective view. Figure 13 shows how the building block is tessellated and scaled to form a plate. This plate has three blocks through the thickness; that is, 9 elements.

Having proposed this 27-element building block my approach has been to develop it in three stages:

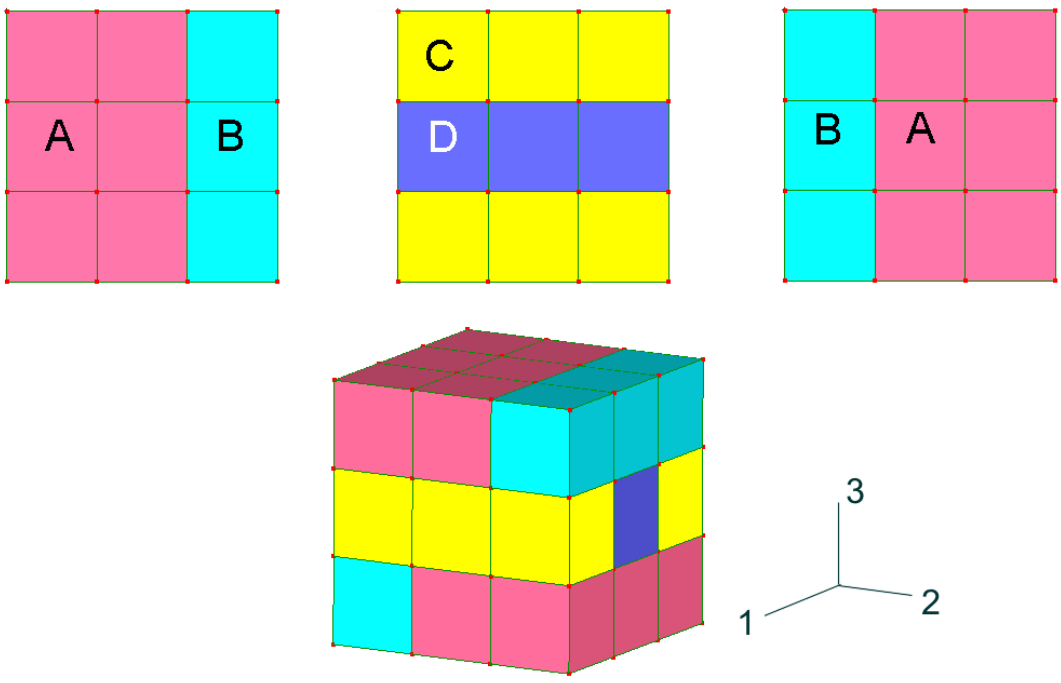

Figure 12: 27-element cube of materials A, B, C, D used as the 'building block' for a 3-D solid quasi-orthotropic material. Upper frames show the three layers of hex20 elements through the thickness.

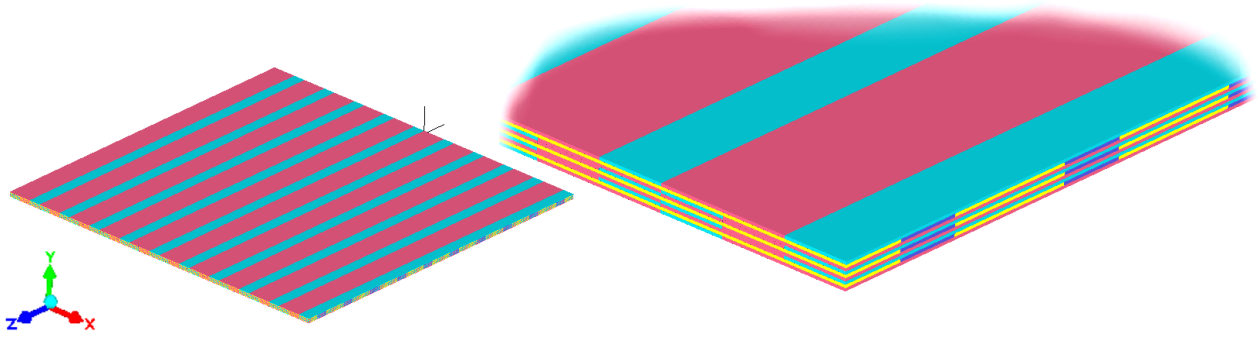

Figure 13: Model of 262 mm square plate. The detail shows the three layers of the basic 27-element cuboid through the thickness, y direction.

1. develop an analytical formula which allows calculation of values of the four Young's moduli, E_A, E_B, E_C, E_D, so that four macro elastic constants $E_1 = E_{||}$, $E_2 = E_{\perp}$, $G_5 = G_{||}$, $G_4 = G_{\perp}$ of Table 2 are matched fairly closely,

2. optimise these values in some way so that LISA produces as good a match as seems possible to the resonant frequencies and vibrational patterns of a square plywood plate, used as a calibration reference,

3. apply the model, thus optimised on the reference square, to other plywood plates of different sizes and shapes and make comparisons with experiment.

In practice two approaches to optimisation have been followed. One was applied to a model with three blocks, 9 elements through thickness, and is descibed in the next section. The other was applied to a model with only one block, 3 elements, through thickness and is described in §10.

7.2 Spring approximation to elastic constants

The first task, therefore, is to develop formulae for the first estimate of values. This is made using a 'combining springs' set of simultaneous equations analogous to Eq 15. Note that E_3, Young's modulus in the through thickness direction, will feature even though I have not been able to measure it. Adjustment of E_3 will be a way to alter G_4 and G_5, though the precise relation of E_3 to the shear moduli is not analytically determined.

The choice of whether to add the springs which represent E_A *etc.* in series or in parallel must observe the constraint that the finite elements remain joined at all their nodes as they stretch. This means that the springs must first be treated in groups of nine, in layers perpendicular to the direction of applied force, and so added in parallel. Subsequently the three layers along the direction of force are added in series. Accordingly I introduce this notation: in calculating E_1 the combined modulus of the front layer (along the direct of force) is E_{11}, of the middle layer is E_{12} and of the back layer is E_{13}, and similarly for E_2 and E_3. To simplify the notation further, let A stand for E_A, *etc.*. We therefore obtain

$$E_{11} = E_{13} = \tfrac{1}{9}(4A + 2B + 3C), \qquad E_{12} = \tfrac{1}{9}(4A + 2B + 3D) \tag{16}$$

$$\frac{1}{E_1} = \frac{1}{3E_{11}} + \frac{1}{3E_{12}} + \frac{1}{3E_{13}}$$

$$E_{21} = E_{23} = \tfrac{1}{9}(3A + 3B + 2C + D), \qquad E_{22} = \tfrac{1}{9}(6A + 2C + D)$$

$$\frac{1}{E_2} = \frac{1}{3E_{21}} + \frac{1}{3E_{22}} + \frac{1}{3E_{23}}$$

$$E_{31} = E_{33} = \tfrac{1}{9}(6A + 3B), \qquad E_{32} = \tfrac{1}{9}(6C + 3D)$$

$$\frac{1}{E_3} = \frac{1}{3E_{31}} + \frac{1}{3E_{32}} + \frac{1}{3E_{33}}$$

Measuring in GPa we require $E_1 = 10{\cdot}2$, $E_2 = 3{\cdot}46$. E_3 is unknown, though we suppose it to be small, less than E_2. I choose a starting value of 1 and find solutions to the above simultaneous equations using a computer algebra package. As examples, for $E_3 = 1$

$$\text{Set } D = C. \text{ Then } A = 1{\cdot}88, \quad B = 41{\cdot}62, \quad C = 0{\cdot}349,$$

$$\text{Set } D = 2C. \text{ Then } A = 1{\cdot}88, \quad B = 41{\cdot}62, \quad C = 0{\cdot}262.$$

and for $E_3 = 0{\cdot}1$

$$\text{Set } D = 2C. \text{ Then } A = 2{\cdot}04, \quad B = 41{\cdot}77, \quad C = 0{\cdot}0251, \quad \text{Material M3},$$

$$\text{Set } D = 3C. \text{ Then } A = 2{\cdot}04, \quad B = 41{\cdot}77, \quad C = 0{\cdot}0201.$$

The very large ratio of E_B to E_C is quite remarkable.

G_4 and G_5 are determined by using the solution set as input to LISA simulations of beam torsion. Similar simulations of beam bending and stretching can be used to check the values of E_1 and E_2 for the composite material. Of course, Poisson's ratio does not feature in Eq 16 so in the first instance I take $\nu_B = \nu_B = \nu_C = \nu_D = 0{\cdot}3$. Figure 14 is an example of a bend model for E_2, and Figure 15 a torsion model for G_5. These were calculations for material M3 above. When used in Eq 11 and 12 respectively, they give $E_2 = 3{\cdot}11$ GPa, fairly close to the experimental value, but $G_5 = 0{\cdot}53$ GPa is too large.

The setting up and running of LISA static models to iterate all the elastic constants has proved quite a time consuming process. The highest order 3D element in LISA is the 20 node

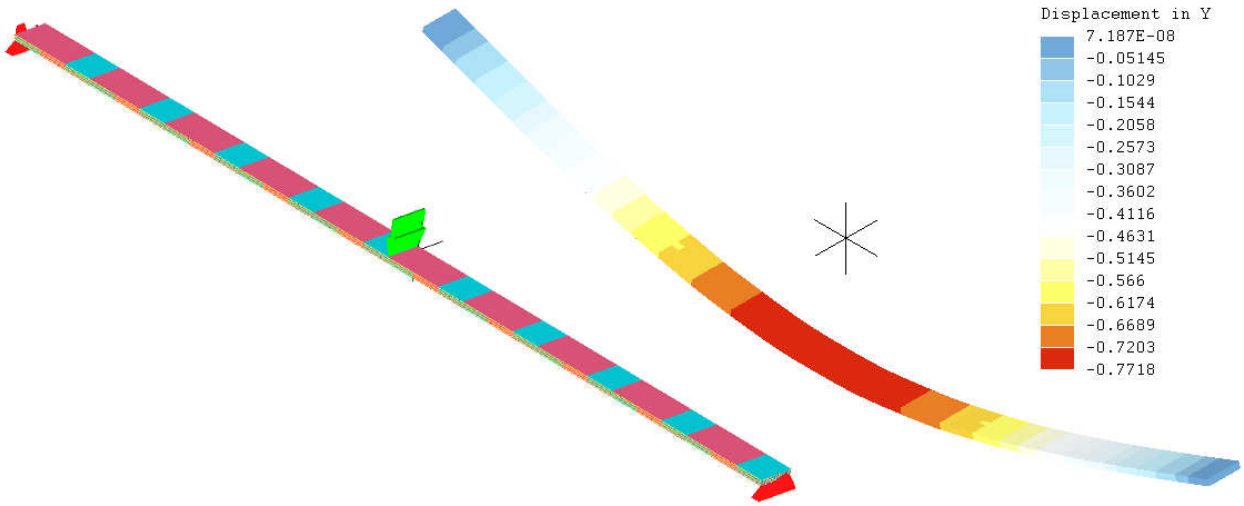

Figure 14: LISA screen displays showing quasi-orthotropic beam in 3-point bending to determine E_2 (left), and predicted deflection (right).

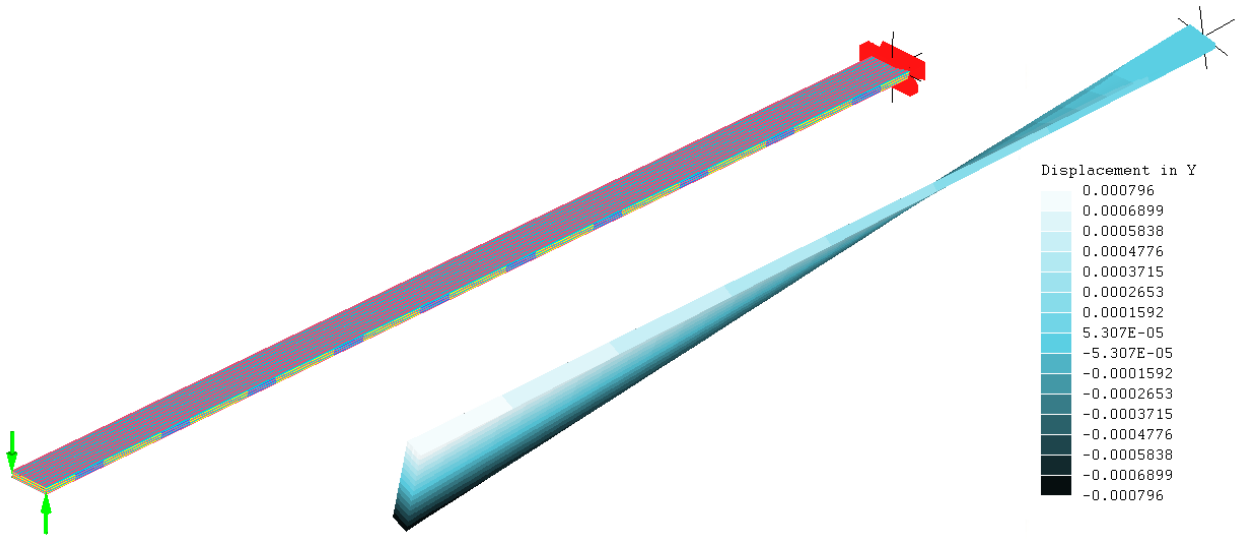

Figure 15: LISA screen displays showing quasi-orthotropic beam in torsion to determine $G_{||} = G_5$ (left), and predicted twist (right).

'hex20' and a key question is 'How many elements are required to achieve convergence?' – which we trust will be to the physically correct values! The traditional way of answering this question is to repeat the calculation with increasing refinements of mesh. However, a limit is soon reached set by computer memory for a 32-bit program. To retain the quasi-orthotropic properties, the 27-element building block must be tessellated in its entirety to model a beam or plate. Suspecting that several elements would be required through the thickness, I started with three blocks, making the beam or plate 9 elements deep. This limited the number of blocks across the surface area, $x - z$ plane, to about 10 by 10 (30×30 elements). In later numerical explorations, described in §10, the number of blocks through thickness has been relaxed to two and then one (6 or 3 elements), allowing somewhat finer meshing over the plate's surface.

For a few examples, Table 6 summaries the elastic constants of five quasi-orthotropic materials. M3 was the example cited above. M4, M4a and M4b differ only in Poisson's ratio, which is the same for all four constituent materials A, B, C, D. For M5 E_A and E_B have been adjusted significantly to make this material have constants close to the experimental values. Since the latter are subject to experimental uncertainty, I consider that searches for an even closer fit to the four statically determined elastic constants is not worthwhile. Rather these candidate materials should be input into dynamic models, and a significant number of predicted normal modes compared with experiment. This, after all, has been the object of developing an orthotropic model.

Material ID	E_A	E_B	E_C	E_D	ν	E_1	E_2	G_5	G_4
M3	$2 \cdot 037$	$41 \cdot 775$	$0 \cdot 0251$	$0 \cdot 0502$	$0 \cdot 3$	$10 \cdot 53$	$3 \cdot 11$	$0 \cdot 531$	$0 \cdot 679$
M4	$2 \cdot 043$	$41 \cdot 780$	$0 \cdot 0176$	$0 \cdot 0351$	$0 \cdot 3$	$10 \cdot 46$	$3 \cdot 02$	$0 \cdot 459$	$0 \cdot 556$
M4a	$2 \cdot 043$	$41 \cdot 780$	$0 \cdot 0176$	$0 \cdot 0351$	$0 \cdot 1$	$10 \cdot 49$	$2 \cdot 94$	$0 \cdot 543$	$0 \cdot 652$
M4b	$2 \cdot 043$	$41 \cdot 780$	$0 \cdot 0176$	$0 \cdot 0351$	$0 \cdot 45$	$10 \cdot 44$	$3 \cdot 49$	$0 \cdot 413$	$0 \cdot 505$
M5	$2 \cdot 423$	$40 \cdot 000$	$0 \cdot 0176$	$0 \cdot 0351$	$0 \cdot 35$	$10 \cdot 23$	$3 \cdot 50$	$0 \cdot 475$	$0 \cdot 562$

Table 6: Effective elastic constants of various quasi-orthotropic materials as determined by FEA-simulated bending and torsion tests. The model is based on the 27 element cube in Figures 12, 13, 14 and 15.

8 Modelling normal modes of plywood reference square

8.1 First estimate compared with experiment

The calibration reference specimen was the same 262 mm plywood square described in §6.2. Since material M5 has elastic constants quite close to the values in Table 2, it can be our first choice for modelling normal modes. The results are summarised in Table 7.

Material M5		n				
	m	0	1	2	3	4
FEA 3D	0			199	484	829
Expt				*206*	*566*	*1080*
	1		71	236	516	849
			55	*240*	*603*	*1114*
	2	116	180	349	603	939
		127	*163*	*334*	*664*	*1198*
	3	312	362	523	771	
		354	*388*	*520*	*816*	
	4	577	631	760		
		692	*726*	*834*		
	5	896	930			
		1142	*1180*			

Table 7: Comparison of resonant frequencies of a 262 mm square plywood plate as modelled as material M5 using the 3D finite elements of Figure 13, and determined experimentally (italics).

This 3D model is prone to Out of Memory errors due to its large size (8100 elements). Hence the number of modes which can be determined is limited; on a 32 bit operating system, Windows XP, up to 17 modes can be determined, this rising to 25 on the 64 bit Windows 7 system. Since 3 or 4 or these modes are body translations and/or rotations, the number of relevant, deformation-only modes is 21.

Comparison of Tables 4 and 7 shows that overall the agreement with experiment is considerably better with the 27 element 3D model than with the 2D model of §6.2, although the agreement for the beam-like $m-0$ and $0-n$ modes is distinctly poorer. Various measures of goodness of fit can be proposed. Since pitch is perceived as ratios of frequencies, I have opted for the single measure

$$Q \;=\; \sum_{modes} \left(\frac{f_{FEA}}{f_{expt}} - 1 \right)^2 \;; \tag{17}$$

that is, the sum of squared fractional errors. On this measure material M5 scores 0·48 over the 21 relevant modes. Over the same modes the 2D model of §5.2 scores 3·13. This comparison seems enough for us to conclude that the 3D, 27 element model with material M5 parameters is a moderately successful orthotropic model for plywood.

Naturally these questions quickly arise:

1. How good a match can be found by varying the input parameters?
2. What is the most efficient way to determine a 'best' set of input values?
3. Does this model, optimised on a 262 mm plate, give equally good results on plywood plates of other sizes, including ones with curved edge?
4. Do the best input parameters remain the best when the size and number of elements are changed – that is, are the material parameters peculiar to a particular meshing of the component?
5. Can an equally accurate but smaller model be made with less than 3 composite blocks through the thickness?

8.2 Optimisation by gradient search

The first two questions are closely related. The goodness of fit will be measured by Q, Eq 17. Then a 'best' fit to experiment involves minimising Q as a function of the 8 parameters E_A to E_D, ν_A to ν_D. I say 'a' best fit rather than 'the' best fit because we do not know the form of the hypersurface Q, nor indeed whether it is continuous. Since it takes about 15 to 20 minutes to set up, run and record LISA for each material, the convergence scheme should require as few evaluations as possible. Nevertheless, one must accept that 10 to 20 will be needed.

I have examined a steepest gradient method, on the assumption that Q is a smooth, continuous function [5]. Initially I have taken the four Poisson's ratios to be equal, thus reducing the minimisation of Q to a search over 5 dimensions. From an initial material definition, vary one of the independent variables E_A, E_B, E_C, E_D, ν at a time and calculate an approximation to each partial derivative by, for example,

$$\frac{\partial Q}{\partial E_A} \approx \frac{Q_1 - Q_0}{E_{A1} - E_{A0}}, \tag{18a}$$

where Q_0, E_{A0} refer to the starting values and Q_1, E_{A1} to the perturbed values. I chose about a 4% change in the Young's moduli and a 10% to 20% change in ν because of its smaller influence. The maximum gradient from the starting position is defined by $\mathbf{grad}\, Q$. Within this local linear approximation, the minimum of Q should lie somewhere along the line of maximum gradient, whose components are given by

$$E_A(k) = E_{A0} - k\frac{\partial Q}{\partial E_A}, \tag{18b}$$

and similarly for the other four independent variables. Here k is a small positive parameter specifying points along the line. We do not know the value of k at which the minimum of Q is most closely approached, so I have evaluated Q for two non-zero values, k_1, k_2. The three points $Q(0)$, $Q(k_1)$, $Q(k_2)$ then lie on a straight line (in the space spanned by E_A, ... ν) which should contain the minimum of Q. I have estimated the position of this minimum by fitting a parabola through these three points and finding its minimum. This occurs at the value of k which, in Eq 18b, gives the required improved values of E_A *etc.* and hence an improved material. From there the process can be iterated until no worthwhile further improvement is obtained.

Table 8 give numerical value for the partial derivatives at M5. Clearly the Young's moduli of the central layer in the 27 element cuboid of Figures 12 and 13 dominate. Table 9 uses these partial

[5] An alternative approach to finding a good fit is described in §10 for a one-block thick model. This gives further insight into the dependence of Q on the input Young's moduli A, B, C, D.

derivatives in Eq 18b with $k = 0{\cdot}0005$ and $0{\cdot}001$. The parabola through $Q(k)$ for materials M5, M6, M7 has a minimum of $0{\cdot}329$ at $k = 0{\cdot}0012$. Thus $k = 0{\cdot}0012$ defines material M8 which is closer to the optimum than starting material M5.

	M5	vary A	vary B	vary C	vary D	vary ν
$A = E_A$	2·423	**2·52**	2·423	2·423	2·423	2·423
$B = E_B$	40	40	**41·5**	40	40	40
$C = E_C$	0·0176	0·0176	0·0176	**0·0183**	0·0176	0·0176
$D = E_D$	0·0351	0·0351	0·0351	0·0351	**0·0365**	0·0351
ν	0·35	0·35	0·35	0·35	0·35	**0·28**
Q	0·480	0·465	0·466	0·469	0·472	0·487
$\partial Q/\partial A$ etc·		−0·16	−0·01	−15·22	−5·49	−0·10

Table 8: Calculation of partial derivatives $\partial Q/\partial A$, *etc.* local to material M5. The values that have been varied are highlighted in bold.

material	M5	M6	M7	M8
k	0	0·0005	0·001	0·0012
A	2·423	2·423	2·423	2·423
B	40	40	40	40
C	0·0176	0·0252	0·0328	0·0359
D	0·0351	0·0379	0·0406	0·0417
ν	0·35	0·35	0·35	0·35
Q	0·480	0·385	0·339	0·329

Table 9: Fitting a parabola to points $Q(0)$, $Q(0{\cdot}0005)$ and $Q(0{\cdot}001)$ (materials M5, M6, M7) to determine minimum at $k = 0{\cdot}0012$ (M8).

I carried out a further stage of iteration starting from M8, finding again that C and D have the largest effect, though with ν having some significance. A and B had almost no effect on Q. The effect of ν is to change the normal frequencies such that modes appear in a somewhat different order. Much of the fractional error in Q is contributed by the lowest mode, 1-1. For most material specifications this frequency is close to 73 Hz. However there are sets of values of the independent variables at which it drops abruptly to about 53 Hz, close to the experimental 55 Hz. The effect is to cause a jump in Q from about $0{\cdot}32$ down to about $0{\cdot}19$. (One could argue that Q is too course a measure to discern these finer changes in modal frequencies.) The best fit is with material M10 with specification

$$A = E_A = 2{\cdot}425, \quad B = 40{\cdot}0, \quad C = D = 0{\cdot}04632, \quad \nu = 0{\cdot}3525$$

and has $Q = 0{\cdot}188$. It is remarkable that both constituent materials C and D have the same elastic constants, making the central layer in Figure 12 uniform and isotropic. I have investigated the changes in modal frequencies and hence in Q when only one of the four Poisson's ratios is changed and find that almost all effect is due to ν_B. Table 10 gives the modal frequencies of the optimum material: compare with Tables 4 and 7. Considering the experimental uncertainties and the small effect of frequency shift on perceived pitch for all but the lowest notes, the agreement is acceptable.

The above procedure for arriving at some optimum material may seem very involved and tedious, but bear in mind that a procedure something like this would be required even if the finite element program did supply genuine 2D orthotropic shell elements. The reason is that nine elastic

Material M10		n				
	m	0	1	2	3	4
FEA 3D	0			203	521	936
Expt				*206*	*566*	*1080*
	1		53	246	561	957
			55	*240*	*603*	*1114*
	2	112	191	375	658	1071
		127	*163*	*334*	*664*	*1198*
	3	324	384	571	862	
		354	*388*	*520*	*816*	
	4	619	691	841		
		692	*726*	*834*		
	5	991	1031			
		1142	*1180*			

Table 10: Comparison of resonant frequencies of a 262 mm square plywood plate modelled as optimised material M10 and determined experimentally (italics).

constants or their equivalents must be input to any orthotropic model. Some can be determined by direct static tests as in §5.1, but others require sophisticated methods, including determining them from measured normal modes. At least one attempt to determine elastic constants of orthotropic plates by modal analysis has been published : L. Deobald and R. Gibson, *J. Sound & Vibration* 1988, **124(2)**, pp 269-283.

8.3 Weaknesses in the model

The model has not given as close a fit to the experimental values for plywood as did the LISA 2D sheet model for the aluminium plate of §3. By comparison, it is a poor approximation, but not so poor as to be of no use in acoustic studies. Two significant shortcomings are apparent:

1. The M10 material, optimised for modal frequencies, does not give the best match to the elastic constants as determined by static methods. Using the simulated methods for Young's modulus by bending and shear modulus by twisting (Figures 14 and 15), M10 has

   $$E_{||} = E_1 = 10 \cdot 35, \quad E_{\perp} = E_2 = 3 \cdot 71, \quad G_{||} = G_5 = 0 \cdot 64, \quad G_{\perp} = G_4 = 0 \cdot 82 \text{ GPa.}$$

   The shear moduli are respectively 40% and 50% larger than the experimental values (Table 2). I am unable to explain why, though it may be related to the difficulty of achieving the frequency of the lowest mode, 1-1.

2. There is a frequency dependent inconsistency to the variations $\partial Q/\partial A$, $\partial Q/\partial B$, etc. in the optimisation algorithm. In Eq 18 a, b the goodness-of-fit value Q is the sum over 21 resonances. If instead we split the modes into three groups according to frequency, it becomes clear that the lowest modes behave quite differently from the highest ones. The trends are shown in Table 11 for small variations in $A = E_A$ etc. about material M8, a stage just before reaching M10. It

Band	$\frac{\partial Q}{\partial A}$	$\frac{\partial Q}{\partial B}$	$\frac{\partial Q}{\partial C}$	$\frac{\partial Q}{\partial D}$	$\frac{\partial Q}{\partial \nu}$
< 300 Hz	+	+	+	+	+
300 - 600 Hz	+	−	−	−	+
600 - 1200 Hz	−	−	−	−	−

Table 11: Direction of change in partial derivatives over three frequency bands for material M8. + denotes an increase, − a decrease.

is not necessary to show the numerical values to see that this is a serious weakness, potentially undermining the whole optimisation algorithm. Clearly a linear elastic system should not have this dispersive behaviour. It implies that the elastic moduli depend of frequency. A similiar effect was commented upon in §6.2, Table 5 for the 2D shell model. I can merely speculate on the source of this undesirable quality; it may come from the increasing difficulty of the finite elements to approximate the increasing curvature of the plate as the number of node lines increases. This being so, it implies that attempts at optimisation should be carried out only over limited spans of frequency, even though this would significantly increase the awkwardness of calculation, increasing the number of LISA runs and requiring a patching together of results.

Even if this frequency dependence did not occur, we could not be sure that material M10 is the overall best approximation to real plywood. The hypersurface $Q(A, B, C, D, \nu)$ may have several valleys and hollows. I cannot see how this could be explored except by an exhausting Monte Carlo-type search, perhaps combined with the above minimum-searching procedure. I have had little appetite for such a search, though the alternative optimisation approach in §10 comes close to a brute search using the elastic spring model.

8.4 Effect of changing in-plane size of elements

This subsection gives a partial answer to Question 4 of §7.2.1 regarding the stability of the optimised model to changes in meshing, and to whether M10 remains the best material as mesh sizes are changed. The subsection considers the effect of changing the in-plane (x, z) dimensions of the finite elements; the effect of reducing the number of through-thickness (y) elements is investigated in §10.

The method has been to run LISA several times using the 27-element block model (Figure 13) with material M10. For each run the number of blocks in the x (across grain) direction was reduced in steps from 10, and the elements scaled up to maintain the 262 mm width. Thus 5 blocks implies a scaling by ×2. In all cases there were 10 such blocks (30 elements) in the vertical direction (with grain). The results are presented in Figure 16 for modes up to 2-4.

Perhaps the first thing to note is the anomalously low frequency of 1-1 at 10 blocks wide, the size at which M10 was optimised. We have already remarked how this 53 Hz value is sensitive to the input elastic constants E_A, etc. Since the number of elements is being changed only in the x direction, we might expect modes m-0 to be effected much more than ones 0-n. However, this is not bourne out by the numbers; for example, 0-3 increases as elements are stretched (decreasing number of blocks) whilst 0-4 decreases. Some modal frequencies such as 2-0, 1-3, 3-2 and 1-4 change little. Mode 3-3 shows one of the largest changes between 10 blocks and 5 – from 862 Hz to 915 Hz – but this is only a semitone in pitch. I also made one calculation reducing the number of blocks in the grain direction from 10 to 8; the numbers of 27-element blocks were $8 \times 8 \times 3$. The change from the $8 \times 10 \times 3$ mesh of blocks was negligible – no more than 1 Hz in any mode. In general it seems

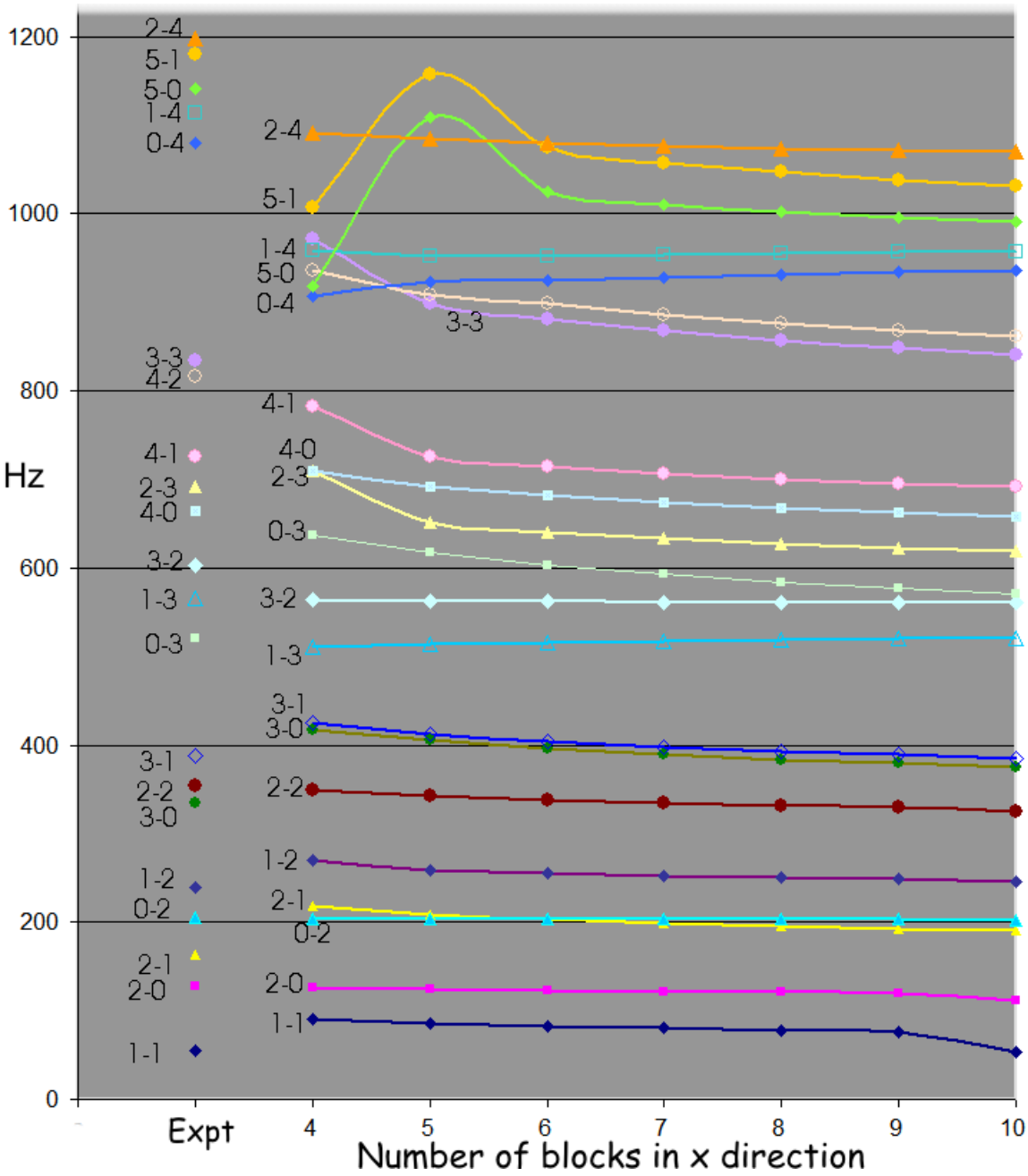

Figure 16: Effect of in-plane mesh stretching on modal frequencies predicted by LISA for 262 mm plywood square. Horizontal axis shows number of 27-element M10 blocks in x direction to make the 262 mm width. The experimental values are shown on the left.

that a scaling up by about 50%, corresponding to a reduction in the number of elements to about 60%, does not greatly affect the predicted frequencies of most modes, and does not alter the order of modes.

9 Application of 27-element model to other plywood specimens

This section addresses question 3 in the list of §7.2.1. One critical test of the model optimised on the reference sequare is whether it adequately predicts the normal modes of other lamella made of the same Far Eastern plywood.

9.1 Large rectangle 262×370 mm

At the beginning of this study I investigated a plywood rectangle 262 mm along the grain by 370 mm across, mean thickness $3 \cdot 57$ mm. It was from this that the 262 mm square of §5 was cut. My technique was less developed at that early stage and clearly measurements cannot now be repeated. Nevertheless tap tones were recorded and several Chladni figures obtained, as presented in Figures 1 to 4 in §2. The corresponding calculations with LISA, material M10, have been made in two ways:

1. by scaling the x, cross-grain direction by 370/262, thus staying with the $10 \times 10 \times 3$ mesh of 27-element blocks, requiring a mesh of 8100 elements in total, $30 \times 30 \times 9$.

2. by keeping almost the same dimensions for each element, but adding four more 27-element blocks in the x direction to extend to 370 mm ($14 \times 10 \times 3$ blocks, $42 \times 30 \times 9$ elements).

The stretching method 1 is clearly equivalent to that of §8.3.

Comparison is given in Table 12 together with the few experimental results. Because of the 32 bit memory limitations already mentioned, the second method, with added elements, could only calculate 8 useful modes. Agreement between the two FEA methods is sufficiently close not to be of practical concern, and for several modes the agreement with experiment is good. This is consistent with the study in §8.3 so overall I consider these results satisfactory.

	Stretched	Added	
Mode	Hz	Hz	Expt
1-1	56	53	
2-0	61	60	64
2-1	129	123	99
3-0	167	164	173
0-2	203	204	208
1-2	232	229	232
3-1	236	227	
2-2	304	296	268
4-0	330		333
4-1	387		
3-2	421		441
0-3	521		
5-0	529		564
1-3	536		
4-2	572		
5-1	588		
2-3	609		608

Table 12: Application of optimised material M10 to 262 by 370 mm plywood rectangle. The headings Stretched and Added denote the two methods of extending the 262mm model to 370×262 mm.

9.2 Small rectangle 108×262 mm

This rectangle was the off-cut when the 262 mm square was sawn from the original 262 by 370 mm specimen. The spectra of taps tones again pointed out the frequencies to investigate for Chladni figures. A collection of photographs is shown in Figure 20 overpage, arranged to compare with Figure 8 for the plywood square.

Experimentally I found it quite difficult to obtain good quality figures for some modes, such as 1-4. Even where quite sharp Chladni figures appeared, for some modes an ambiguity remained as to which frequency is the 'pure' resonance. Figure 17 illustrates this for the 2-2 mode; I have taken 920 Hz as the most likely because the crossing lines are almost straight.

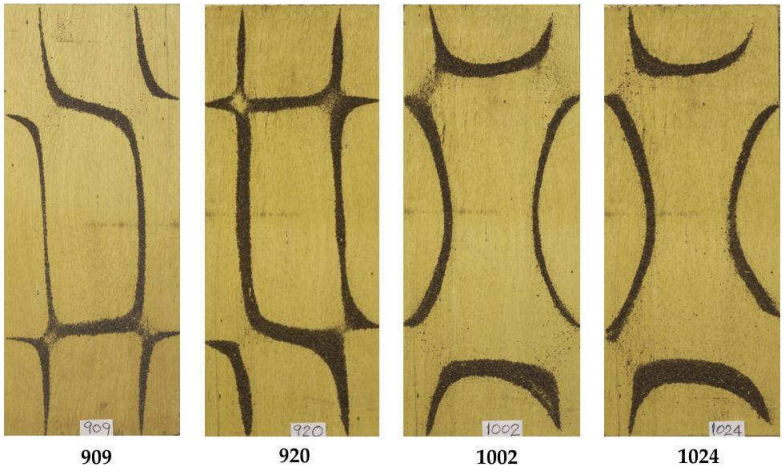

Figure 17: Chladni figures near mode 2-2 of rectangle 108×262 mm, illustrating the ambiguity in identifying resonances.

As with the wider rectangle of §9.1, the finite element calculations used scaled (compressed) elements and/or fewer elements in the x, cross-grain direction, with 10 blocks being maintained along the grain. Whilst most of the mode shapes predicted by LISA can be identified clearly, the 2-2 and 0-4 modes show some of the ambiguity seen experimentally in Figure 17. Figure 18 compares the displacement patterns for these two modes as calculated using 10, 6 and 4 27-element blocks in the x direction. For mode 2-2, the leftmost LISA picture (obtained for the 10 elements of the

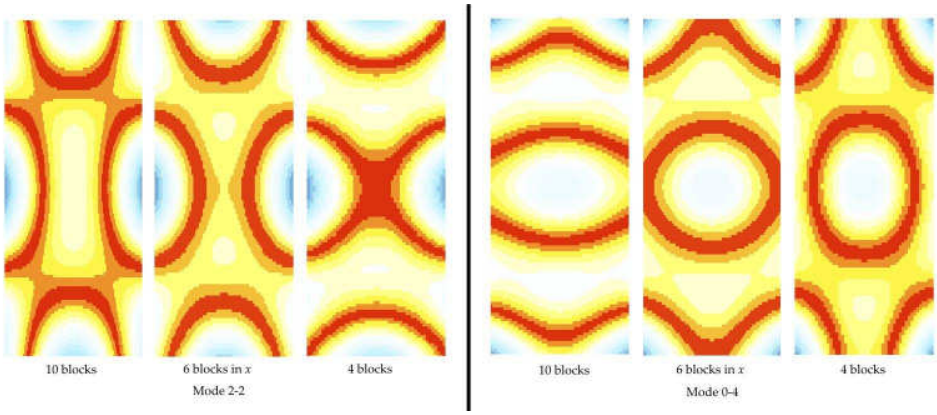

Figure 18: LISA predictions of Mode 2-2 and 0-4 according to three different meshs. Material M10.

original 262mm square compressed across the grain to 108 mm) is similar to the Chladni figures at 909 and 920 Hz in Figure 17. However the central LISA picture, for 6 blocks, looks very like the Chladni figures at 1002 and 1024 Hz. For mode 0-4 no LISA image is as simple and obvious as the experimental figure at 1152 Hz. Indeed the rightmost LISA picture, for 4 blocks, is hardly recognisable as mode 0-4.

The effect of changing the mesh is summaried in the graphs of Figure 19. This corresponds to Figure 16 for the 262mm square, except that for the square the elements were being stretched whereas for the small rectangle they are being compressed. It supports the view that a scaling of up to about 50% makes only a modest change. Overall, however, the agreement between experiment and calculation with material M10 is poorer for this specimen than for either of the larger ones. Modes 0-3, 0-4, 1-2, and 1-4 are way off. It seems that material M10, optimised for the 262 mm square, cannot be the best approximation for the smaller rectangle. This could prompt a systematic search for a better approximation, but I have restricted myself to only three other materials – M4,

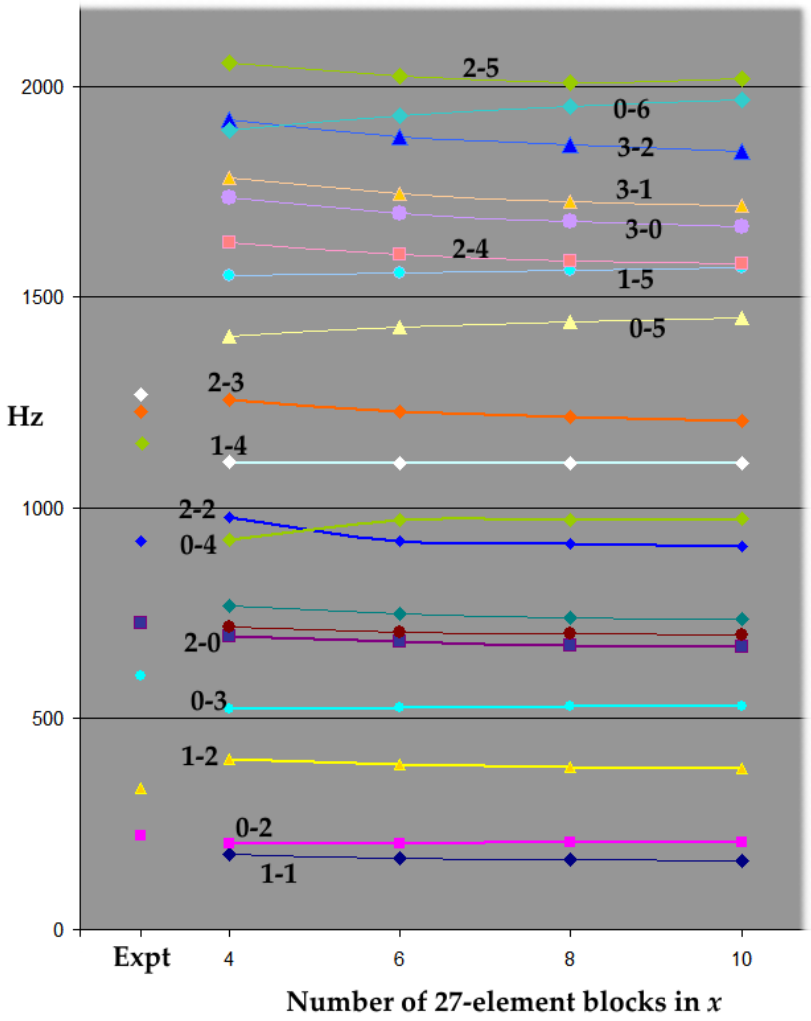

Figure 19: LISA calculations of the modal frequencies of the 108×262 mm plywood rectangle with material M10. The graphs show the effect of changing the number of 27-elements blocks in the x (cross grain) direction.

M5, M8 identified in Tables 6 and 9 as stages in the search for the optimium. For each of these the small rectangle has been meshed with 7 blocks of 27-elements in the x direction, scaled by $\times 0 \cdot 59$. The results are even worse than for M10!

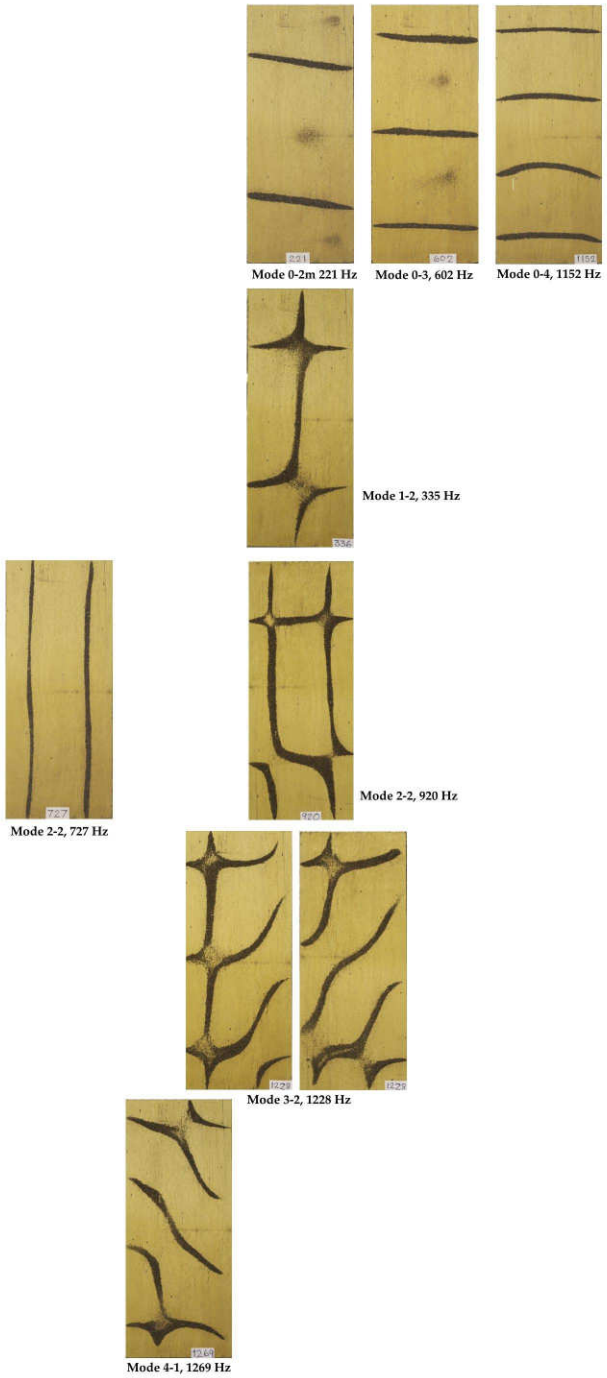

Figure 20: Photographs of Chladni figures of various modes of plywood rectangle 108mm by 262 mm. Surface grain is vertical in pictures.

9.3 Trapezium cut from 262mm square

The next test piece has been made from the 262 mm reference square by cutting a triangle from one side. Figure 21 shows the LISA model made by 'cutting' a triangle from the upper right corner of the 262 mm square model used in §8. This too used material M10. For about 2/3 of modes examined the computed pattern of displacements could be identified with an experimental Chladni figure; these are shown side by side in Figure 22. With the remaining modes there was a general similarity of pattern, but not enough to justify confidence in a match. These unmatched pictures are shown in Figure 23.

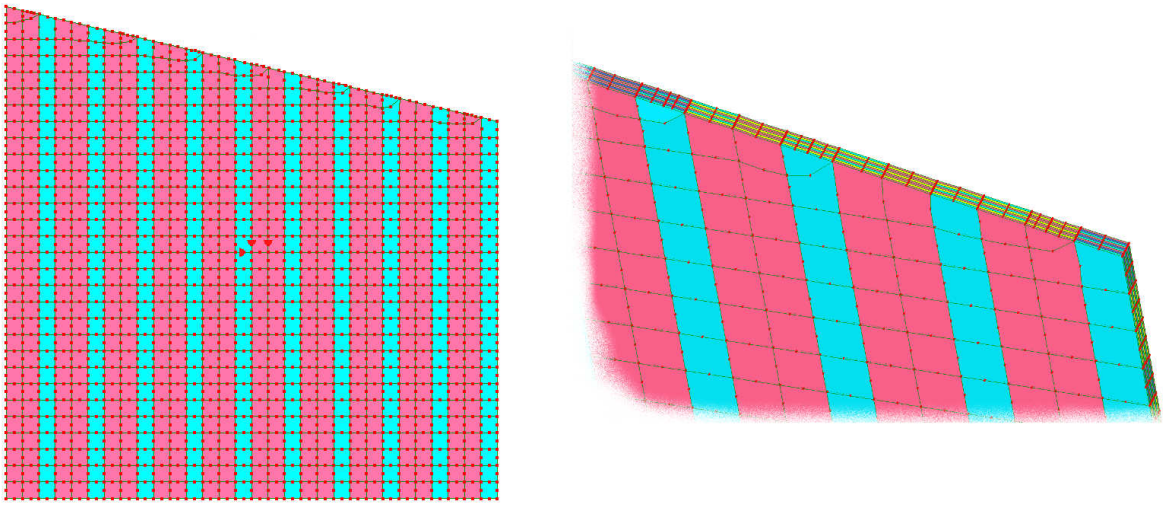

Figure 21: LISA model of plywood trapezium. Left picture shows whole object with elements outlined. Red is material A, blue material B. Right picture is detail of one corner.

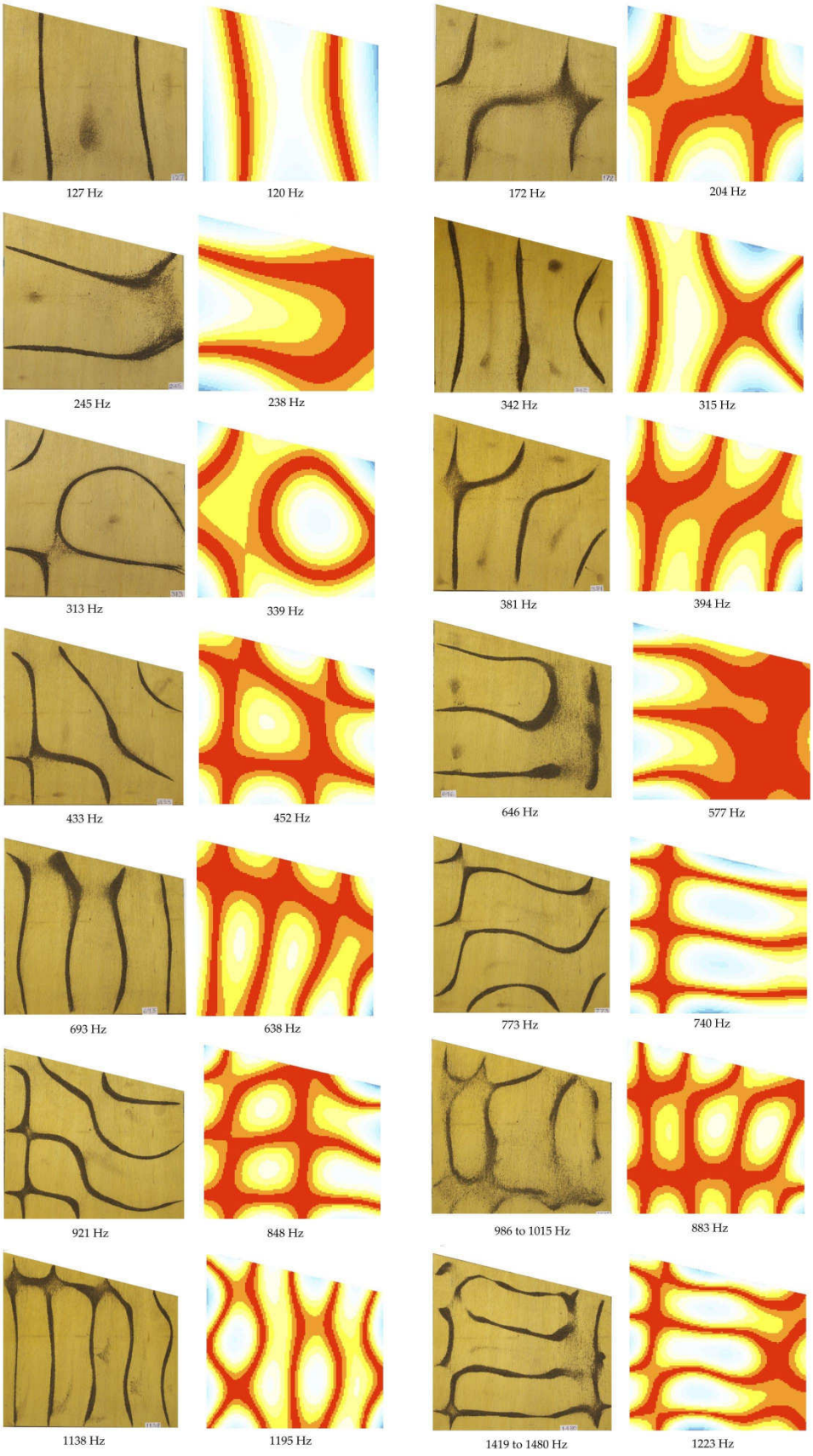

Figure 22: Vibrational modes of a plywood trapezium as determined experimentally and modelled with LISA using the 27-element block model, material M10, 3 blocks (9 elements) through thickness.

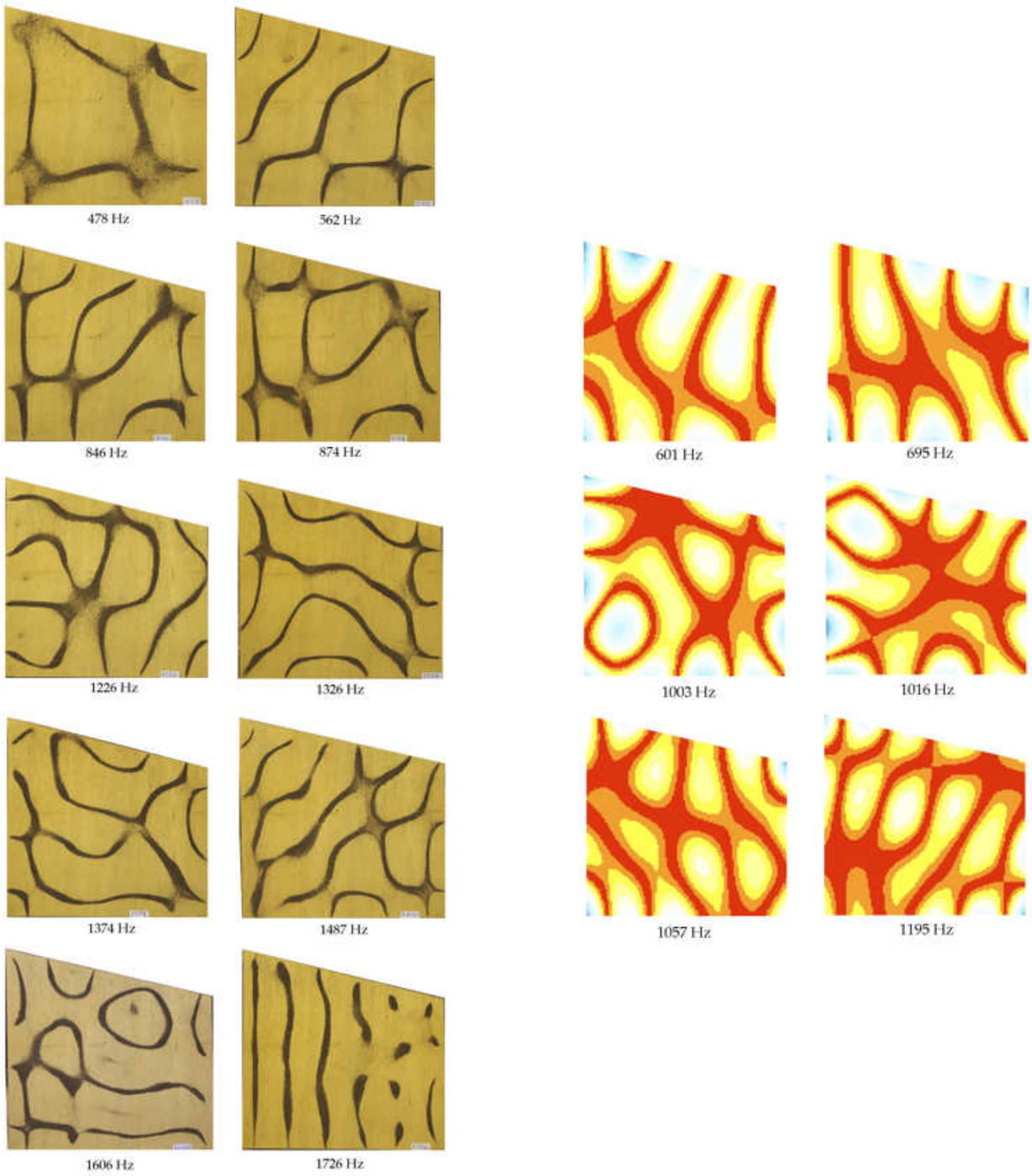

Figure 23: Modes of the plywood trapezium for which a match between experiment and FEA cannot be made with confidence.

9.4 Plate from stringed musical instrument

The final specimen studied is a large flat plate with curved perimeter, representing the top plate of a stringed musical instrument like an asymmetric viola. This was cut from the same sheet of plywood as the other specimens. As previously, tap tones were analysed to pick out peaks in the frequency spectra, and Chladni figures obtained at or close to these resonant frequencies. The lowest peak was at 21 Hz, almost outside the bandwidth of the loudspeaker. It proved difficult to obtain any clear Chladni figure below about 70 Hz; resonance behaviour was manifest through a general shaking of the specimen, but without causing the particles to congregate in any consistent pattern.

In LISA this specimen was modelled essentially by taking the mesh used in §8 for the 262 mm square, adding four more blocks in the grain direction and one block across grain, and then deleting elements which lay wholly or mostly outside the profile of the plate. Finally nodes were moved to bring them onto the perimeter. All 6795 elements remained of the hex20 type. Figure 24 shows the mesh. Note that for this specimen the grain runs horizontally in the pictures, left-right.

There was a slight complication in matching the plywood specimen with the finite element model in that the grains of the two outer layers of the 3-ply were about 8^o out of alignment. I have dealt with this by placing the orthotropic axis in the LISA mesh along the mean direction. Because of the reduced number of elements, 6795 compared with 8100 for the 262 mm square, LISA was able to model up to 36 modes before running out of memory. Material M10 was again used. The 30 lowest modes which involve deformation without rigid body translation or rotation, or in-plane flexing, are illustrated in Figure 25 to 27. In each figure the LISA-computed displacement patterns are compared with photographs of the Chladni figures. I consider agreement on the shapes of the figures to be fairly encouraging. The experiemntal and LISA-calculated modal frequencies are listed in Table 13. Agreement here is not strong, but nor is it too poor to be a useful guide. Note that some of the higher-frequency modes predicted by finite elements are so close together that they could not be resolved in experimental reality.

LISA	Expt	LISA	Expt
29	25	470	500
60	54	507	-
82	72	546	520
100	101	567	560
110	97	597	576
162	128	687	643
204	200	700	697
228	215	705	-
238	226	728	716
286	260	779	737
322	284	785	770
354	331	862	855 - 877
393	370	868	890
433	429	940	948?
457	474	973	988

Table 13: Comparison of calculated and experimental modal frequencies of musical instrument plate, taken from Figures 25, 26, 27. LISA used material M10.

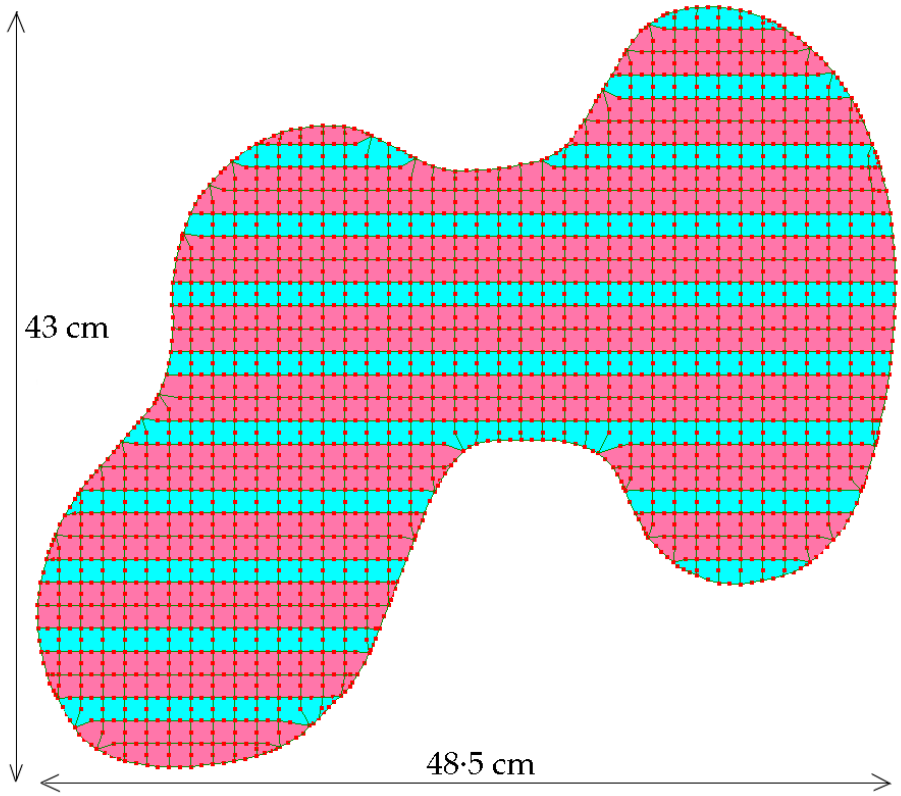

Figure 24: LISA finite elements making up model of flat plywood plate, typical of a stringed musical instrument. The surface grain runs left to right.

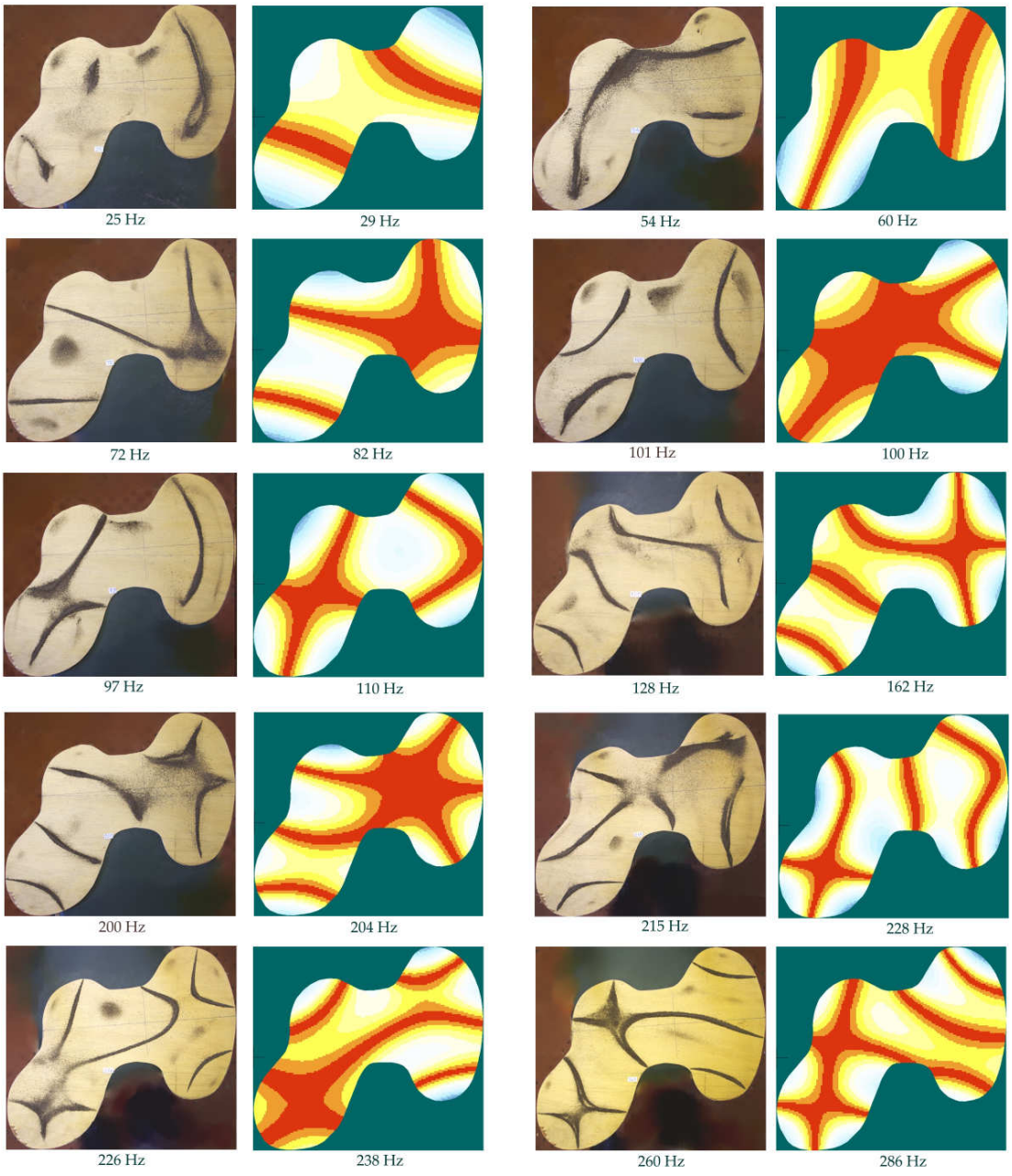

Figure 25: Comparison of Chladni figures and LISA-computed displacement images of lowest frequency normal modes of musical instrument plate. In the LISA images the red areas have nominally zero displacement. Material M10, 27-element block model, 3 layers (9 elements) through thickness.

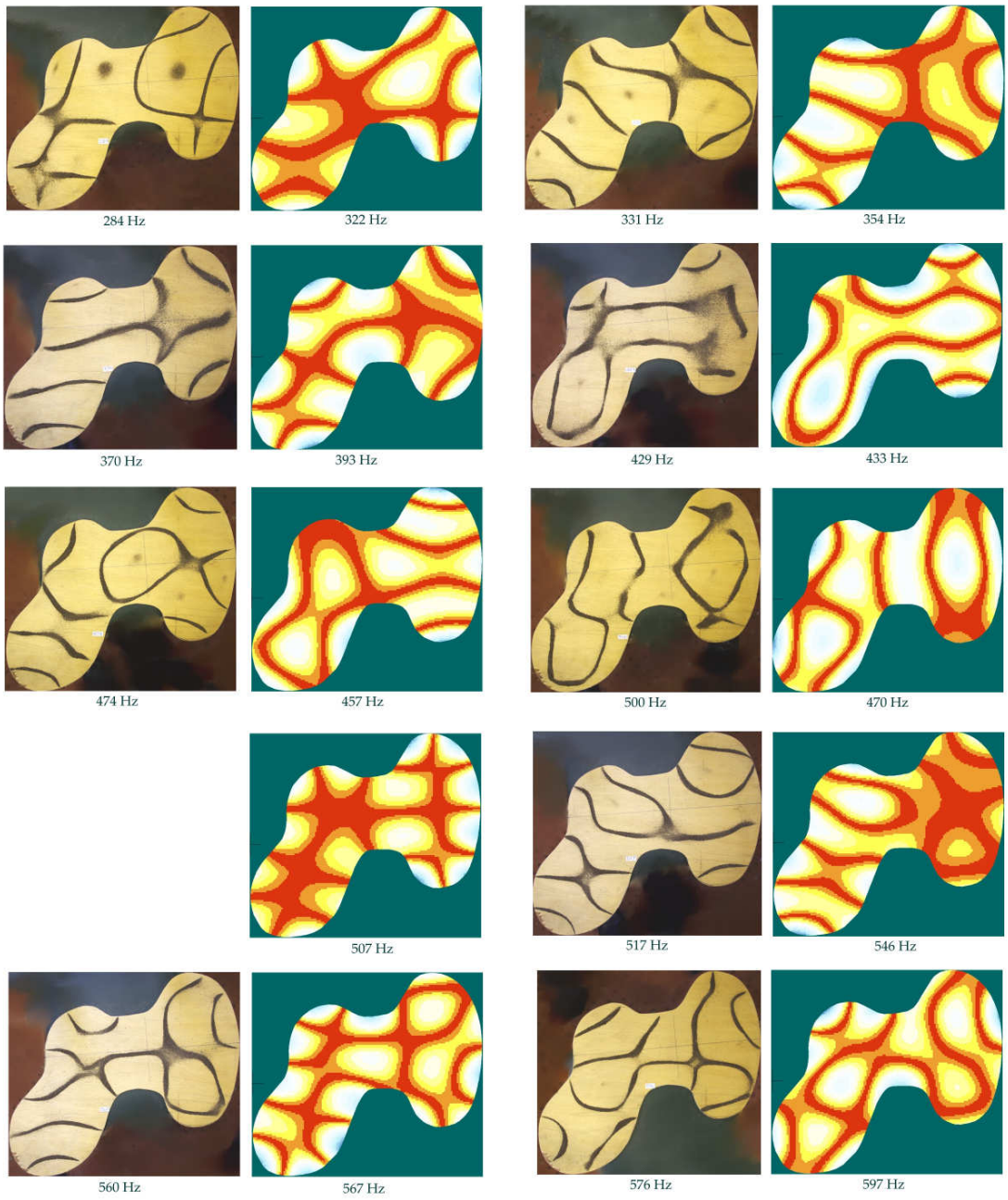

Figure 26: Mid-frequency vibrational patterns of plywood musical instrument plate, continuing from Figure 25.

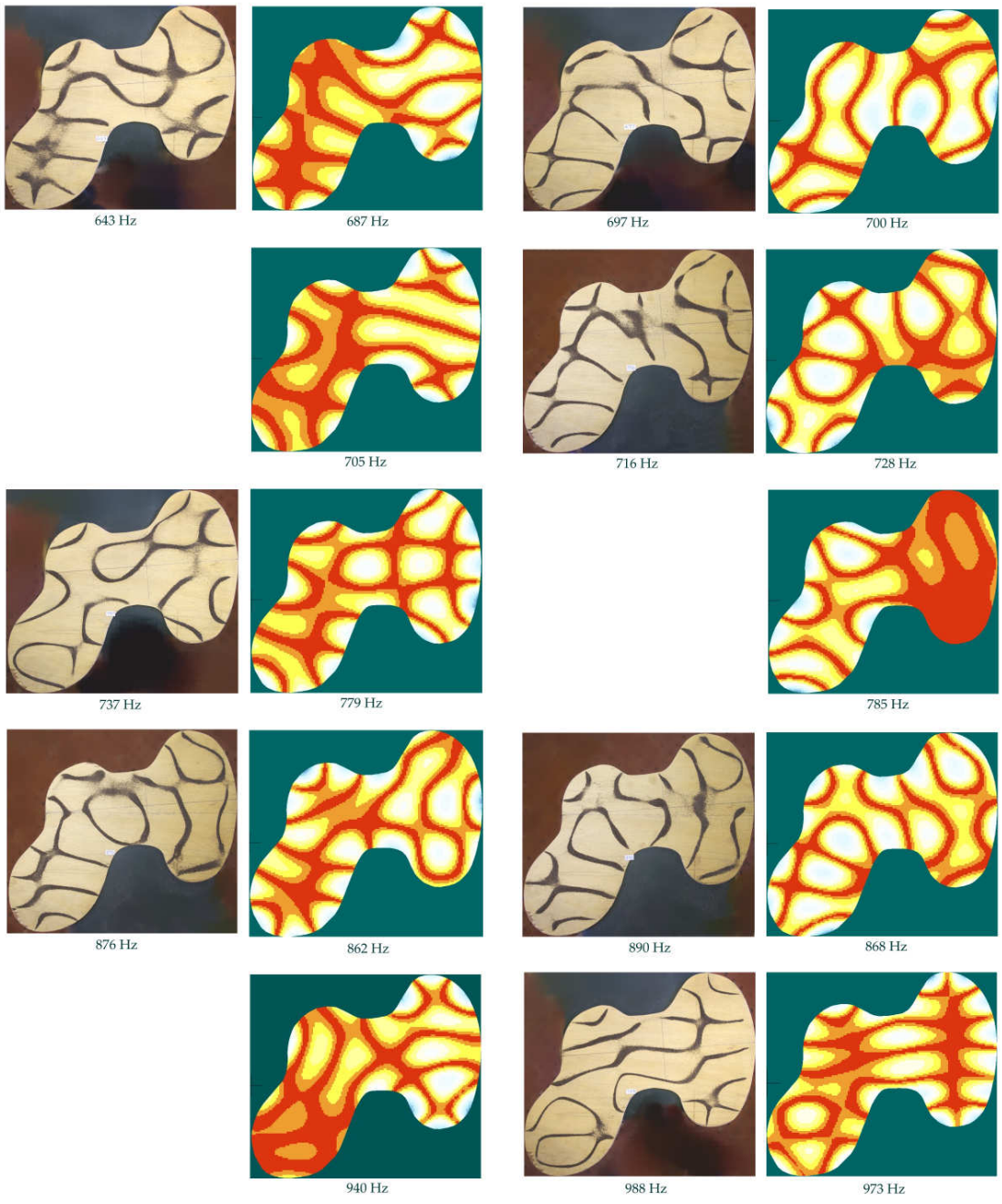

Figure 27: Higher frequency vibrational patterns of plywood musical instrument plate, continuing from Figure 26.

10 Model with 1 or 2 blocks through thickness

All the calculation with the 3D model of §7 have so far used three of the 27-element buiding blocks through the thickness, as illustrated in Figure 13. Because it would be a great calculational advantage to have an effective model with fewer elements, I have made a short investigation of the effect to reducing the number of through-thickness blocks to 2 and 1.

I have also taken the opportunity to explore a different approach to optimising the elastic parameters $A = E_A$, etc. This merely involved using a numerical program to solve the algebraic relations in §7.2, Eq 16 for $E_{||} = E_1 = 10 \cdot 2$ GPa, $E_\perp = E_2 = 3 \cdot 46$ GPa, and various small values of E_3. As with Table 6, I started by guessing $E_3 = 0 \cdot 1$, then $0 \cdot 05$, etc. for $\nu = 0 \cdot 3$. Then ν was also varied to $0 \cdot 4$ and other values. For each such model material I ran LISA for the 262 mm reference square with only 1 block through thickness and calculated a quality Q according to Eq 17, except limiting it to the lowest 16 modes. This limitation was because

1. we have noted a frequency dependence to the goodness of fit, and the lowest frequencies are the most important to musical instruments,
2. LISA predicted unphysical in-plane modes at high frequencies (seen only in the 1-block model).

In the numerical solutions the values of A and B varied very little from about $2 \cdot 04$ and $41 \cdot 8$ respectively. E_3 changed C and D. One could vary the ratio $C : D$, but for a given value of E_3 this ratio made hardly any difference to the quality Q – I found this surprising. A consequence of this was that C could be set almost to zero, with all the elastic stiffness of the middle layer being supplied by the strips of material D! The best material determined by this trial-and-error approach, called R1, has parameters

$$A = 2 \cdot 0375, \qquad B = 41 \cdot 775, \qquad C \approx 0, \qquad D = 0 \cdot 10044 \text{ GPa}.$$

C was set to 5000 Pa to avoid any potential instabilities in LISA's matrix solving algorithm.

Having thus optimised R1 on the 262 mm reference square, I applied it to the musical plate specimen, with both 1 block and 2 through thickness. I also applied the M10 material, optimised for 3 blocks, to the same plate with 2 and 1 blocks. All these results are summarised in Table 14. The Q value at the foot of the table shows perhaps surprisingly that M10 gives better results on a 2-block model than on the 3-block model for which it was optimised. Of course, we could not have known this in advance. The R1 model gives almost as good results, though it is stable only for the modes listed. I have examined the shapes on the Chladni figures calculated by LISA for these five models and find them remarkably similar and consistent – they all look as Figure 25, 26, 27. This is very heartening.

11 Summary and Conclusion

I have wanted to model the vibration of wooden plates, but using the available finite element program LISA v7.7.1 which is restricted to dynamic models with only isotropic materials. I have attempted to approximate orthotropic behaviour using an assembly of isotropic finite elements. Initially a 2D shell approximation was examined in §6, but found to be a poor fit to all modes except the m-0 and 0-n types. I therefore developed a 3D model based on a $3 \times 3 \times 3$ block on hex20 elements, attempting to optimise the fit to the resonant frequencies of a square plywood reference plate. The starting point for estimating the input parameters has been numerical solution of analyitic equations for an assembly of springs in series and parallel.

Expt	Material	M10	M10	M10	R1	R1
	No. of blocks	3	2	1	2	1
	Optimised?	Y				Y
25		29	27	29	24	27
54		60	59	65	54	61
72		82	77	84	70	78
108		100	97	106	88	98
97		110	106	116	98	109
128		162	154	165	135	151
193		204	196	212	173	193
215		228	222	239	196	216
226		239	231	250	207	229
260		286	272	291	236	262
284		322	310	332	271	300
331		354	340	365	299	330
370		393	379	403	325	357
429		433	423	454	371	406
474		457	445	476	391	426
500		470	466	490	402	438
-		507	486	515	411	452
517		546	525	558	449	491
560		567	548	580	464	508
576		597	582	611	493	
643		687	665	701	544	
697		700	681	710	565	
		705	687	721	577	
716		728	710	739	593	
	Q, 16 modes	$0 \cdot 20$	$0 \cdot 10$	$0 \cdot 32$	$0 \cdot 19$	$0 \cdot 12$

Table 14: Comparison of resonant frequencies in Hz of musical instrument plate for the M10 and R1 model materials and various number of 27-element blocks through the thickness. The quality parameter Q is calculated for the lowest 16 modes. The third row in the header indicates whether the material was optimised for that number of blocks.

Suspecting that many elements through the thickness would be required to model plate dynamics with any accuracy, I have carried out a series of calculations using 3 blocks, 9 elements through thickness, this being the maximum number of elements which the 32-bit LISA program could cope with. The model has been moderately successful, but suffers from a significant weakness in that the elastic moduli seem to be frequency dependent. Finally I examined a reduced model with only 1 block, 3 elements through thickness, optimising the properties for frequencies less than 400 Hz on the 262 mm square reference plate. The simpler 1-block model has given fairly good agreement with experiment over the lowest 16 modes. Although agreement with experiment is not nearly as good as for the aluminium plate of §3, I consider the quasi-orthotropic model in LISA 7 adequate for investigating some acoustic aspects of stringed musical instruments.

John Coffey, August 2012.
The author can be contacted via mathstudio.co.uk.